Distribution of NMHC Ratios in the Pacific During PEM-West B and PEM-Tropics A

by

Christopher Chay Casso

Submitted to the Department of Earth, Atmospheric, and Planetary Sciences in Partial Fulfillment of the Requirements for the Degree of

Bachelor of Science

at the

Massachusetts Institute of Technology

June 2000

Signature redacted

Signature of Author .....
Department of Earth, Atmospheric, and Planetary Sciences
May 25, 2000

Signature redacted

Certified by .....
Reginald E. Newell
Professor of Earth, Atmosperic, and Planetary Sciences
Thesis Supervisor

Signature redacted

Accepted by .....
Timothy L. Grove
Chairman, Undergraduate Thesis Committee

Distribution of NMHC Ratios in the Pacific During PEM-West B and PEM-Tropics A

by

Christopher Chay Casso

Submitted to the Department of Earth, Atmospheric, and Planetary Sciences
on May 25, 2000 in Partial Fulfillment of the
Requirements for the Degree of Bachelor of Science in
Earth, Atmospheric, and Planetary Sciences

ABSTRACT

Under the auspices of NASA's Global Tropospheric Experiment (GTE), the Pacific Exploratory Missions (PEM) have collected numerous air samples of many regions of the troposphere. Data from PEM-West B (February 7 to March 15, 1994), and PEM-Tropics A (August 15 to October 5, 1996) have been used here to study non-methane hydrocarbon (NMHC) ratios and to compare pollution transport by large scale convection and subsidence, as well as horizontal transport across the Pacific. For PEM-Tropics A, 7 cases are studied, each involving different aspects of transport. Persistent circulation features in the South Pacific played a significant role in NMHC ratio distribution and processing. For PEM-West B, sources of a large pollution region are studied and compared to equatorial transport. NMHC ratios were found to be useful tracers of pollution distribution through the troposphere. The contrasts of these ratios across relatively small distances, particularly on either side of the South Pacific Convergence Zone in PEM-Tropics A, suggest that convection shapes pollution transport and distribution, particularly in the South Pacific.

Thesis Supervisor: Reginald E. Newell
Title: Professor of Earth, Atmospheric, and Planetary Sciences

TABLE OF CONTENTS

1. INTRODUCTION

The Pacific Exploratory Missions (PEM) have provided an extensive collection of data concerning tropospheric airflow and pollution distribution [Hoell et al., 1996, 1997, and 1999]. One major goal of the PEM missions is to observe and analyze atmospheric chemistry and airflow across spring and fall seasons in both hemispheres. Data for the South Pacific in particular have been sparse; the PEM-Tropics missions allow a significant amount of useful analysis of photochemistry in relatively pollution-free regions. The missions so far have flown near east Asia in the winter (PEM-West B), a time of maximum outflow from the continent and overall subsidence over the continent; near east Asia in the summer (PEM-West A), a time of lesser outflow from the continent and considerable convection over land and sea; and two sets of flights covering the South Pacific from New Zealand to South America (PEM-Tropics A and B), which included measurements across the South Pacific Convergence Zone (SPCZ) and the Intertropical Convergence Zone (ITCZ). The PEM measurement data is archived with other GTE missions through the Internet at GTE's web site, http://www-gte.larc.nasa.gov/.

The South Pacific Convergence Zone (SPCZ) significantly factors in lower tropospheric circulation features for the PEM-Tropics A time period. A convenient summary and analysis of much of the literature concerning the SPCZ, including its seasonal variability, is provided by Vincent [1994]. This concentrated region of convection, stretching from approximately the Philippines southeast through Tahiti in the PEM-Tropics A period [Fuelberg et al., 1999], separates two anticyclonic regions, generally centered around Australia and Easter Island, respectively. The southeastern portion of the SPCZ is more variable, consisting of frontal-related temperature gradients, and the SPCZ in fact terminates near 150°W in diagrams by Fuelberg,

among others, for this reason. However, this region of variable temperature gradients is theorized here to be crucial for overall airflow transport analysis.

Nonmethane hydrocarbons consist of predominantly land-based emissions, such as fossil-fuel and biomass burning, most of which can be classified as anthropogenic. During atmospheric transport in the troposphere, NMHCs naturally decompose due to reactions with $OH^{\cdot}$ and $NO_3^{\cdot}$ In general, the larger the hydrocarbon, the easier it is to decompose into other hydrocarbons. Alkanes (RH) produce alkyl peroxy (RO_2) radicals, which in turn react to produce peroxides, alkyl nitrates, peroxynitrates, and carbonyl species (adapted from Seinfeld and Pandis, 1998):

$$RH + OH^{\cdot} \rightarrow R^{\cdot} + H_2O$$
$$RH + NO_3 \rightarrow R^{\cdot} + HNO_3$$
$$R^{\cdot} + O_2 + M \rightarrow RO_2^{\cdot} + M$$
$$RO_2^{\cdot} + NO \rightarrow RO^{\cdot} + NO_2$$
$$RO_2^{\cdot} + NO \rightarrow RONO_2$$
$$RO_2^{\cdot} + NO_2 + M \rightarrow ROONO_2 + M$$
$$RO_2^{\cdot} + HO_2^{\cdot} \rightarrow ROOH + O_2$$
$$RO^{\cdot} + O_2 \rightarrow R'CHO + HO_2^{\cdot}$$
$$HO_2^{\cdot} + HO_2^{\cdot} \rightarrow H_2O_2 + O_2$$

Tracking NMHC transport can provide a useful method of understanding airflow and constituent transport in the atmosphere. However, the NMHCs must have a significant atmospheric lifetime in order to be tracked over a long period, limiting most analysis of NMHCs to ethane (C_2H_6), ethyne (C_2H_2), and propane (C_3H_8). The two NMHC ratios most commonly used for analysis are C_3H_8 / C_2H_6 and C_2H_2 / CO, due to their high correlations in biomass burning and emissions from fossil fuel [Talbot et al., 1997]. Recent lifetimes for these constituents are given for the tropics as well as for global conditions [Singh and Zimmerman, 1992]; for C_3H_8, C_2H_6, and C_2H_2 these are 5.3, 20 and 6.7 days for the tropics and 22, 92 and 24 days for the globe as a whole. Shorter lifetimes came from the higher $OH^{\cdot}$ assumed in the tropics (a factor of 10). NMHC ratios are used here to attempt to track transport of pollution across the

Pacific troposphere. McKeen and Liu [1993] used computer modeling to find that atmospheric mixing played a significant role in determining NMHC ratios, undermining an absolute determination of tracking air parcel times from the source with ratios alone. In this paper, trajectories and streamlines will be used in conjunction with ratios to track the progression of air regions over time. While exact origins of air parcels cannot be determined, spatial variability in the data will be noted here.

This paper is meant to provide specific examples of NMHC ratio measurements made over the Pacific Ocean, and relate differences in spatial distribution with prevailing atmospheric conditions. Individual NMHCs over the Pacific Ocean have been discussed previously for PEM-West A [Blake et al., 1996], PEM-West B [Blake et al., 1997], and PEM-Tropics A [Blake et al., 1999]. Smyth et al. [1996] discussed analysis of NMHC ratios and their correspondence with other pollution tracers in PEM-West A. NMHC ratios have also been previously discussed in PEM-West B and PEM-Tropics A [Gregory et al., 1997 and 1999]. In particular, Gregory noted that the NMHC ratios were a definite indicator of the difference in air masses over certain areas of the Pacific noted by divergent wind patterns, particularly across the ITCZ and SPCZ. Board et al. [1999] tracked possible origins of air parcels in PEM-Tropics A measurements by using O_3, nitrogen compounds, H_2O_2, CH_3COOH, CH_3OOH, ^{7}Be and ^{210}Pb, and made some comparisons of these data with the C_2H_2/CO ratio. Accuracy for the NMHCs used here is considered to be 5%, with a nominal precision of 1% or 2 pptv [Hoell et al., 1999].

2. APPROACH TO ANALYSES

Data available from PEM-West B and PEM-Tropics A for NMHCs were used in this study. Tracks for these flights can be found in Stoller et al. [1999]. Longitudinal regions were selected

for optimal coverage of mission data and meridional cross-sections were prepared. These regions were further divided into segments of 4 degrees latitude by 2 km altitude. Data collected at a boundary line were included in the segments above and to the north of the data point. These data were combined for each mission over several flights to form coherent longitudinal mission slices. With this approach, some features may be blurred by time changes in a region occurring between flights, e.g. the time difference between the PEM-Tropics A Tahiti-Hawaii profiles between DC-8 Missions 3 and 19, which were carried out on September 3, 1996 and October 5, 1996, respectively. For these figures, east-west transport between missions was neglected. Figures were created for the mean and standard deviation of the segments in each slice. All data points were included in the mean calculations; boxes with less than 3 data points were omitted from the standard deviation calculations.

Because of the nature of these flights, some data at ground level may be biased toward the airports where the airplanes land. This might be more significant in the northern PEM-West B flights, where the airports are often in or near highly polluted urban regions [Blake et al., 1997].

3. NMHC RATIOS IN PEM-TROPICS A

Three longitudinal strips were studied for this mission. The locations were chosen to parallel the main segments of the PEM-Tropics A mission. Data from the DC-8 New Zealand and Fiji flights, 170°W-170°E (Missions 12, 13, 14, 15, 16, 17, and 18) are shown in Figure 1 [see Hoell et al., 1999, for mission dates]. Data gathered in the flights to and from Tahiti and Hawaii, 140°W-160°W (DC-8 Missions 4, 6, 7, 10, 11, 12, 18, 19; P-3B Missions 10, 11, 12, 13) are summarized in Figure 2. DC-8 Mission 5, while in the Tahiti region, did not gather enough NMHC samples to be included here. Data from the flights near Easter Island, 100°W-120°W

(DC-8 Missions 7,8,9,10; P-3B Missions 13,14,15,16) are shown in Figure 3. Due to the oscillation of the SPCZ and the rapid convection and subsidence of the air in certain areas around the South Pacific, averaging vertical and horizontal airflow in the that region across the time period of the PEM-Tropics A mission resulted in no net vertical airflow across portions of this unstable region. As a result, sample 5-day averages of stream flow (Figure 4) and vertical motion (Figure 5) are included to better demonstrate this activity, particularly in the region of the SPCZ. Many of the airflow features noted in this paper were consistent for the whole of PEM-Tropics A.

Before NMHC data can be compared, a baseline of background ratio levels must be established. The region with the smallest NMHC ratios over the PEM missions lies at the northern end of the 170°E-170°W profile in PEM-Tropics A, near the boundary layer from 12°S to the equator, between the SPCZ and the ITCZ. C_2H_2/CO ratios reach approximately 0.2-0.4 pptv/ppbv and C_3H_8/C_2H_6 ratios reach about $3.0x10^{-2}$-$5.0x10^{-2}$ pptv/pptv in this region. Given the pollution from biomass burning and industrial activity farther west in Indonesia and the Philippines and north from more industrialized nations, it is safe to assume these values are close to the minimum across the Pacific region for the PEM-Tropics A period. Measurements in a similar region during PEM-West B Mission 6 showed mostly equal or higher ratios than PEM-Tropics A, though one C_2H_2/CO area was measured as low as 0.11 pptv/ppbv. The possible reasons behind this lower value are discussed below with PEM-West B.

3.1. Case 1: Easterly Equatorial Subsidence

Streamlines at 850 hPa over the Pacific during PEM-Tropics A (Figure 4a) show a long stretch of easterly equatorial winds below a height of approximately 6 kilometers, proceeding

through a region of high $OH^{\cdot}$ production, with a transport time of approximately 15-20 days from the South American coast to near Fiji. The vertical motion (Figure 5) shows subsidence across this area. (See Fuelberg et al. [1999] and Blake et al. [1999] for representative trajectories in this region, particularly the back trajectories terminating at 700 millibars in Fuelberg for DC-8 Missions 4, 15, and 16, as well as P-3B Mission 17.) A single thin line outlines this equatorial region in Figures 1, 2, and 3. This also corresponds with the aged marine airmass category in Board et al. [1999]. Because the airflow in the equatorial region is consistent subsidence, it can be assumed that atmospheric mixing was less of a factor in the distribution of the NMHC ratios here compared to areas farther south. Following this region along the stream flow from east to west, the C_2H_2/CO ratios decrease steadily from approximately 0.65 pptv/pptv north of Easter Island (Figure 3a) to 0.40 near Christmas Island (Figure 2a) to 0.30 north of Fiji (Figure 1a). While not as significant, there are also signs of a gradual decrease in the C_3H_8/C_2H_6 ratio, from $5.1x10^{-2}$-$8.2x10^{-2}$ pptv/pptv north of Easter Island (Figure 3b) to $5.1x10^{-2}$-$6.6x10^{-2}$ near Christmas Island (Figure 2b) to $3.3x10^{-2}$-$5.3x10^{-2}$ near Fiji (Figure 1b). Because of the differences in time between these measurements, a direct comparison cannot be made between these numbers. Nevertheless, they suggest that tropical $OH^{\cdot}$ concentrations steadily process air proceeding through this corridor, leaving the air in the vicinity of Fiji relatively free of pollution.

The eventual distribution of air cleaned through this slow equatorial transport is somewhat unclear. Ozone and PV studies by Newell et al. [1997] suggest that convection by the ITCZ and SPCZ may carry this low-ozone, clean air from the equatorial boundary layer far away from its origin. One possible SPCZ case is described below in Case 3; an ITCZ case will be described further in the discussion of PEM-West B.

3.2. Case 2: Mid-level New Zealand Jet/Australia Anticyclone

This region, outlined by dashes in Figures 1 and 2, shows airflow from around 850 hPa entering the anticyclonic region and the relative homogeneity of this area suggests that this air possibly gets trapped inside of this anticyclone. This air in general was more polluted than the equatorial air in Case 1, with a notable increase in C_2H_2/CO values, but was less polluted than that measured in PEM-West B, below. Back trajectories from approximately 6 kilometers at 44°S suggest that a possible origin of this region might have been biomass burning off the east coast of Africa [Board et al., 1999].

The tracking of this outlined region from the 160°W-140°W profile is difficult. The streamlines at 850 hPa in this region (Figure 4a) show part of this difficulty, as some of this air might be caught in the Australian anticyclone and circulate north and west toward the north coast of Australia, emerging in the tropical easterlies there; other parcels of this air could be caught in the SPCZ and drawn eastward to the Easter Island anticyclone and, eventually, South America. Because it is difficult with trajectories alone to track air parcels across regions of sharp convection, such as the SPCZ, air transported into the Easter Island anticyclone is treated as a separate case below.

3.3. Case 3: SPCZ Convection and Transport

Strong SPCZ convection may also explain the contrast in NMHC ratios on either side of the SPCZ [Gregory et al., 1999], as the air directly south of the SPCZ has not been processed by $OH^{\cdot}$ nearly as much as air to the north of the SPCZ, described in the first case above. The sharp contrast between air in the Australian anticyclone to the south of the SPCZ and the $OH^{\cdot}$-processed air to the north is best demonstrated by the ozone lidar profile of DC-8 Mission 16

(Plate 1). This flight, north from Fiji, shows a contrast in the ozone profiles on either side of 15°S, as the SPCZ convection in that area keeps the two airmasses relatively separate. The NMHC ratios show a marked decrease from south to north, suggesting that the SPCZ may mix the two airflows together within its convection. The region of likely SPCZ convection and mixing is outlined with a bold line in Figures 1 and 2.

The SPCZ may act as a possible conduit for airflow coming through the Australian anticyclone. The air from this anticyclone continues into the 160°W-140°W profile south of 16°S, where it may enter the SPCZ and be convected upward. Upper level winds (Figure 4c) show that air above this convection show a marked westerly component, thus carrying any air convected within the SPCZ into the region of the Easter Island anticyclone. There is some evidence in the NMHC ratios that may support this. The area denoted in Figure 2 parallels to some extent the description of some layers observed near Tahiti by Stoller et al. [1999] and Blake et al. [1999]. The 2 kilometer x 4 degree latitude resolution of the boxes in this paper are not enough to distinguish fine-scale resolution of layer structure, particularly when it was found in Stoller et al. that these layers were as thin as 1 kilometer in depth. However, the C_3H_8/C_2H_6 ratio values higher than 6 kilometers between 16°S and 12°S in Figure 2 show larger overall values, similar to a region of low ozone shown in lidar profiles in Stoller et al. [1999]. Similarly, the C_2H_2/CO values in Figure 2 between 4 and 8 kilometers, 20°S-12°S, show elevated values, in the region of high ozone in these profiles. However, the C_2H_2/CO values are lower above 8 kilometers, suggesting that this area might be a separate airmass from the higher C_3H_8/C_2H_6 region.

3.4. Case 4: Elevated Polar Boundary Layer Propane

The region outlined with double lines in Figure 1 is unusual because of its southern location, from 56°S to the Antarctic coast. This data was only measured in one flight, DC-8 Mission 13, and may not be as representative of normal conditions as other data in these longitudinal profiles.

The C_2H_2/CO ratio in this region is higher than equatorial measurements (1.1 pptv/ppbv compared to 0.3), but not more than other regions; however, the C_3H_8/C_2H_6 ratio here (10-15x10^{-2} pptv/pptv) is notably above values elsewhere in PEM-Tropics A, with higher deviations than other measurements in these flights. The numbers are more consistent with northern hemispheric air (see the analysis of PEM-West B below) than southern hemispheric air, which has less industrial activity, and thus less propane output. The origin of the air in this region is difficult to determine, though it is unlikely that the increased propane originated from the Antarctic region. The streamlines included here (particularly Figure 4a) and some trajectories (Fuelberg, unpublished) suggest that this elevated propane might be due to surface-level northerly winds from Australia.

Although the origin of this pollution is unclear, there are some implications as to where it may have traveled. Other similar regions of elevated C_3H_8/C_2H_6 ratios were intercepted during flights south of Tahiti (Figure 2b) and south of Easter Island (Figure 3b). Both possible regions are outlined in dashed lines in these figures, suggesting that perhaps these high levels of C_3H_8/C_2H_6 might have mixed with airflow originally from the area of the Australian anticyclone (see case 2 above).

3.5. Case 5: Air Inside the Easter Island Anticyclone

Measurements from the region near Easter Island (Figure 3) represent the convergence of three different air masses: an airflow south of 20°S, flowing east from Australia and Southeast

Asia [Fenn et al., 1999]; a more northerly flow from the east with an origin off the western coast of South America, circulating around the Easter Island anticyclone; and a flow from the north theorized to have come from off the coast of Central America, intercepted during DC-8 Mission 8 at 9.5 kilometers [Blake et al., 1999, and below].

Much of the circulation around this anticyclone takes place in skies clear of mid-level cloud cover, where photochemical reactions can take place. We suggest that such anticyclonic regions may be treated as some of the "washing machines" of the atmosphere where pollution can be efficiently oxidized. The potential from photochemical activity is amplified, as there were some thin stratocumulus clouds present in part of the region, giving an effective two-way path for the solar radiation.

3.6. Case 6: Interception of Central American Pollution

During DC-8 Mission 8, a flight to the north of Easter Island, a small area of highly polluted air was intercepted at 9.5 kilometers. This area contained some of the highest levels of NMHCs in the PEM-Tropics A mission: methane was measured at 1758 ppbv, ethane at 1149 pptv, propane at 265 pptv, ethyne at 73 pptv, n-butane at 22 pptv, and isobutane at 14 pptv. Other notable constituents, including ozone (66 ppbv) and CO (77 ppbv), were elevated in this region. The elevated propane and butane levels in this area, reflected in the propane/ethane ratio, suggest that this pollution is primarily from fossil fuels; trajectories [see Blake et al., 1999] suggest this air was quickly convected from the surface by the ITCZ near the coasts of Panama and Columbia, and carried southwest from there. The elevated hydrocarbons might have resulted because of unburned natural gas and liquefied petroleum gas [e.g. Blake and Rowland, 1995].

3.7. Case 7: Elevated Propane Near Christmas Island

Another small area of note was measured during P-3B Mission 10, just north of the equator near the boundary layer. The level of propane sharply increased for a short period of time, affecting the C_3H_8/C_2H_6 ratio in that area (noted with bold dot-dashed lines in Figure 2b). Measurements were taken in this area around 00:45 GMT on September 1, 1996, at approximately the same time as a ship's plume of pollution was noted from the flight deck of the P-3B. It is also possible that propane burning from local islands in the region was also a factor in this sudden increase in the ratio. Thus, this box should be discounted from comparisons with the surrounding region.

4. FUTURE STUDIES IN THE SOUTH PACIFIC

The effect of the southeastern end of the SPCZ in transport of air masses from both the westerly flow from the Australian anticyclone and the recirculated easterly flow from the Easter Island anticyclone needs to be examined more thoroughly. Trajectories in the region suggest that the SPCZ might act as a "channel" for air entering it, convecting and mixing lower-level air from both anticyclones to a region of more persistent westerly winds in the upper levels. This could allow for a persistent recirculation of air around the Easter Island anticyclone. It is noted, however, that trajectories at this time cannot fully account for regions of large convection, such as the SPCZ. Some trajectories, as a result, suggest outflow from the SPCZ at heights varying from 5 kilometers to as high as 11 kilometers. Streamlines suggest that the former would likely be caught in the subsidence of the Easter Island anticyclone, while the latter would mostly ignore the circulation of this anticyclone and instead would proceed east across South America.

Tracking the amount of airflow in and out of the Easter Island anticyclone could determine the effect of South Pacific circulation features on pollution transport throughout the Pacific.

5. NMHC RATIOS IN PEM-WEST B

Two longitudinal strips were chosen to represent the majority of the PEM-West B region. The first strip (Figure 6), from 120°E-140°E, particularly covers missions in and out of Hong Kong (Missions 13 and 14, as well as parts of Missions 10, 11, 12, 15, and 17). The second strip (Figure 7), from 140°E-160°E, covers missions farther offshore, based from Guam and Japan (Missions 6, 7, 8, and 9, as well as parts of PEM-West B Missions 5, 10, 15, 16, 17, and 18). See Hoell et al. [1997] for corresponding dates for these flights. Mean streamlines for the PEM-West B mission and mean vertical flows are included as Figures 9 and 10. The three cases examined here correspond to those listed in Talbot et al. [1997].

5.1. Case 1: Aged Marine Air

The main example of the measurement of potentially $OH^{\cdot}$-rich marine air was Mission 6, a flight south of Guam, shown south of 12°N in Figure 7. Like PEM-Tropics A, the air in this region was found to have significantly less pollution than other flights in the PEM-West B period. The C_2H_2/CO ratio in this region is equivalent to the lowest PEM-Tropics A measurements, about 0.10-0.40 pptv/ppbv; however, the C_3H_8/C_2H_6 ratio shows less signs of $OH^{\cdot}$ depletion, remaining at the approximate background level of $6.8x10^{-2}$-$11x10^{-2}$ pptv/pptv across a wide area from 12°S to 20°N. This might be due to an increased northerly circulation of polluted air from northern Asia (see Case 3 below), or, alternately, transport from propane emissions at the eastern end of the Pacific, from Central America and the United States. Studies of PEM-West B ozone and potential vorticity also suggest that this relatively clean air enters the ITCZ at

approximately 10°S, and the deep convection within this region distributes this clean air as far north as 20°N [Newell et al., 1997].

5.2. Case 2: Southern Asia Pacific Outflow

At approximately 20°N, a steady westerly flow from Southeast Asia was measured at an altitude of approximately 6-10 kilometers [Merrill et al., 1997]. This area, stretching north to 28°N in Figures 7 and 8, is difficult to distinguish much from surrounding areas. Its slightly elevated C_2H_2/CO ratio (approximately 0.7-2.1 pptv/ppbv) and near-background levels of C_3H_8/C_2H_6 ($7x10^{-2}$-$19x10^{-2}$ pptv/pptv) may suggest that this airflow picked up some biomass burning from convection over Southeast Asia, differentiating it from propane-enriched air both at lower levels of the troposphere and into higher levels farther to the north [Blake et al., 1997].

5.3. Case 3: North Asian Pacific Outflow

North of approximately 20°N, ratios show a steady upward penetration of ground-level pollution with possible origins in China and Japan. This area of high pollution penetrates the middle troposphere at approximately 30°N, and continued to be evenly distributed up to the tropopause at 42°N. This progression is marked by a dashed line in Figures 7 and 8. This region shows similar characteristics to individual NMHC measurements noted by Blake et al. [1997], showing some mixing of surface air with higher levels. The ratios increase to as much as 5.46 pptv/ppbv for C_2H_2/CO and $101x10^{-2}$ pptv/pptv for C_3H_8/C_2H_6, which were the highest such ratios measured in this analysis.

The mean streamlines and winds for this mission (Figure 8) show a general region of low pressure situated off the coast of Japan at approximately 47°N, 152°E, specifically at 850 hPa, decreasing in intensity at higher levels. This low pressure is associated with a general area of

rising motion to the east, as shown by the measured ECMWF mean vertical velocity for the mission at 700 hPa (Figure 9). Regions of subsidence are located near the coastal regions of China, Korea, and Russia. Some of the possible cases of pollution transport from the Asian continent are discussed in Merrill et al. [1997] and Gregory et al. [1997].

Isentropic trajectories show that it is possible that the higher-level pollution might not be of Asian coastal origin, having instead been carried by strong upper-level winds from Russia, or possibly from as far as Europe and North America. One particular indication of a convergence of multiple polluted air flows is the presence of a strong inversion layer between 500-700 hPa, measured by radiosondes over Tateno, Japan [Talbot et al., 1997]. Nevertheless, the northern region shows evidence of pollution transport to higher levels of the troposphere, where upper-level winds could pick up the pollution and transport it across the Pacific.

6. FUTURE STUDIES IN THE NORTH PACIFIC

The foremost problem with analyses in the North Pacific involves the question of origins of the pollution measured. For the PEM-West B period, airflows from Europe, Russia, China, Japan, and Southeast Asia are difficult to separate, particularly in the Pacific boundary layer offshore, where most of these measurements were made. However, the combined outflows are notable when compared to the relatively-clean South Pacific. In addition, it is possible that the mid-level jet could carry this Pacific pollution across the Northern Hemisphere, making tracking of pollution origins difficult at best. It could be valuable to fly aircraft farther inland, to fully measure the extent of long-range pollution transport and compare it to local pollution outflows.

7. CONCLUSION

We have shown the meridional cross-sections of measured NMHC ratios from PEM-West B and PEM-Tropics A. The results presented here clearly show that NMHC ratios can be used to some extent as atmospheric tracers of pollution transport in the troposphere, given a high enough source production of NMHCs and areas of relatively little convection. Data from the PEM-West B mission help trace a possible mechanism for transport of surface pollution to the upper layers of the troposphere through convection, though this is complicated by possible long-range pollution transport. Data from PEM-Tropics A suggest that both the equatorial boundary layer and the SPCZ play important roles in transport of pollution through the area of the South Pacific. The equatorial boundary layer, particularly when combined with flow around a large anticyclone over Easter Island, serves as a method to remove NMHC pollution through persistent exposure to $OH^{\cdot}$-rich air over a relatively long period of time. This leaves the equatorial air near Fiji relatively free of both hydrocarbons and ozone. The SPCZ alternately serves as a barrier between this clean equatorial air and the more-polluted air trapped around the Australian anticyclone and as a method of mixing the two airflows together. Air mixed in the SPCZ will then proceed eastward over the SPCZ, acting as a conduit to pull boundary-level air to higher levels, where prevailing winds will push the air into the area of the Easter Island anticyclone. There is some evidence, particularly in polluted layers near Tahiti, that this is so. While airflow is difficult to track across and out of the SPCZ because of the rapid convection and subsidence, it is suggested that either this air will either descend into the Easter Island anticyclone due to subsidence or, alternately, will proceed at higher altitudes across South America. The amount of air caught by the Easter Island anticyclone's subsidence could determine to a large extent how clean the air is to the east of this anticyclonic region. Alternately, the amount of air caught by the Australian anticyclone, instead of by the SPCZ, could affect the amount of pollution in Australia and

perhaps Southeast Asia. In addition, the intrusion of Central American pollution into the Southern Hemisphere, as measured in DC-8 Mission 8, may indicate that the Easter Island anticyclone could play a larger role in pollution transport, particularly when combined with convection in the ITCZ. Further missions need to be flown, particularly in the SPCZ region, to determine the full extent of airflow interaction in this region and its resultant effect on pollution levels across the South Pacific.

ACKNOWLEDGMENTS

This work was supported by the NASA GTE program under grant NAG1-1758 and NAG1-2173. Yong Zhu supplied the analyzed meteorological maps which used data from the European Center for Medium Range Weather Forecasts (ECMWF). Plate 1 was supplied by Edward V. Browell and Marta Fenn. I thank all these sources.

REFERENCES

Blake, D. R. and F. Sherwood Roland, Urban leakage of liquefied petroleum gas and its impact on Mexico City air quality, *Science*, 269, 953-956, 1995.

Blake, D. R., et al., Three-dimensional distribution of nonmethane hydrocarbons and halocarbons over the northwestern Pacific during the 1991 Pacific Exploratory Mission (PEM-West A), *J. Geophys. Res.*, 101, 1763-1778, 1996.

Blake, N. J., et al., Distribution and seasonality of selected hydrocarbons and halocarbons over the western Pacific basin during PEM-West A and PEM-West B, *J. Geophys.* Res., 102, 28,315-28,331, 1997.

Blake, N. J., et al., Influence of southern hemispheric biomass burning on midtropspheric distributions of nonmethane hydrocarbons and selected halocarbons over the remote South Pacific, *J. Geophys. Res.*, 104, D13, 16213-16232, 1999.

Board, A. S. et al., Chemical characteristics of air from differing source regions during the Pacific Exploratory Mission-Tropics A (PEM-Tropics A), *J. Geophys. Res.*, 104, D13, 16181-16196, 1999.

Fenn, M. A., et al., Ozone and aerosol distributions and air mass characteristics over the South Pacific during the burning season, *J. Geophys. Res.*, 104, 16197-16212, 1999.

Fuelberg, H. E., et al., A meteorological overview of the Pacific Exploratory Mission (PEM) Tropics period, *J. Geophys. Res.*, 104, D5, 5585-5622, 1999.

Gregory, G. L., et al., Chemical characteristics of tropospheric air over the Pacific Ocean as measured during PEM-West B: Relationship to Asian outflow and trajectory history, *J. Geophys. Res.*, 102, 28,275-28,285, 1997.

Gregory, G. L., et al., Chemical characteristics of Pacific tropospheric air in the region of the Intertropical Convergence Zone and South Pacific Convergence Zone, *J. Geophys. Res.*, 104, D5, 5677-5696, 1999.

Hoell, J. M., et al., Pacific Exploratory Mission-West A (PEM-West A): September-October 1991. *J. Geophys. Res.*, 101, 1641-1653, 1993.

Hoell, J. M., et al., The Pacific Exploratory Mission-West Phase B: February-March, 1994, *J. Geophys. Res.*, 102, 28,223-28,239, 1997.

Hoell, J. M., et al., Pacific Exploratory Mission in the tropical Pacific: PEM-Tropics A, August-September, 1996, *J. Geophys. Res.*, 104, D5, 5567-5583, 1999.

McKeen, S. A. and S. C. Liu, Hydrocarbon ratios and photochemical history of air masses, *Geophys. Res. Lett.*, 20, 2363-2366, 1993.

Merrill, J. T., R. E. Newell, and A. Scott Bachmeier, A meteorological overview for the Pacific Exploratory Mission-West Phase B, *J. Geophys. Res.*, 102, D23, 28241-28253, 1997.

Newell, R. E., E. V. Browell, D. D. Davis, and S. C. Liu, Western Pacific tropospheric ozone and potential vorticity: Implications for Asian pollution, *Geophys. Res. Lett.*, 24, 2733-2736, 1997.

Seinfeld, J. H. and S. N. Pandis, Atmospheric Chemistry and Physics: From Air Pollution to Climate Change, John Wiley & Sons, New York, 1998.

Singh, H. B. and P. B. Zimmerman, Atmospheric distribution and sources of nonmethane hydrocarbons, Gaseous Pollutants: Characterization and Cycling, Ed. J. O. Nriagu, John Wiley and Sons, Inc., 177-235, 1992.

Smyth, S., et al., Comparison of free tropospheric western Pacific air mass classification schemes for the PEM-West A experiment, *J. Geophys. Res.*, 101, 1743-1762, 1996.

Stoller, P., et al., Measurements of atmospheric layers from the NASA DC-8 and P-3B aircraft during PEM-Tropics A, *J. Geophys. Res.*, 104, D5, 5745-5764, 1999.

Talbot, R. W., et al., Chemical characteristics of continental outflow from Asia to the troposphere over the western Pacific ocean during February-March 1994: Results from PEM-West B, *J. Geophys. Res.*, 102, 28,255-28,274, 1997.

Vincent, D. G., The South Pacific Convergence Zone (SPCZ): A Review, *Mon. Weather Rev.*, 122, 1949-1970, 1994.

FIGURE LIST

Figure 1. PEM-Tropics A composite meridional cross-section of mixing ratios for (a) C_2H_2/CO and (b) C_3H_8/C_2H_6 for 170°E-170°W longitude. Squares represent the mean of all measured ratios in the area, with the standard deviation listed in italics. Squares with less than 3 data points do not have a listed standard deviation. C_3H_8/C_2H_6 ratio values are multiplied by 100 for clarity in the figure. Case 1 is denoted with a thin line. Case 2 is denoted with a bold dashed line. Case 3 is denoted with a bold single line. Case 4 is denoted with double lines.

Figure 2. Same as Figure 1, but for 160°W-140°W longitude. Case 1 is denoted with a thin line. Case 2 is denoted with a bold dashed line. Case 3 is denoted with a bold single line. Case 7 is denoted with alternating dots and dashes.

Figure 3. Same as Figure 1, but for 120°W-100°W longitude. Case 1 is denoted with a thin line. Case 5 is denoted with a dashed line. Case 6 is denoted with a striped line.

Figure 4. 5-day mean streamlines and winds (m sec^{-1}) at (a) 850 hPa, (b) 500 hPa, and (c) 300 hPa for September 11 – September 15, 1996, corresponding to DC-8 Flights 9 and 10, as well as P-3B Flights 15 and 16.

Figure 5. 5-day mean vertical velocity (0.01 Pa sec^{-1}) at 850 hPa for September 11 – September 15, 1996.

Plate 1. Cross-section of DIAL-derived O_3 mixing ratio along DC-8 Flight 16 north of Fiji on September 28, 1996. The cross-section follows the flight path over time, so it is not a true north-south cross-section. Latitude and longitude are noted at the bottom of the diagram, while ozone (in ppbv) and time (in UTC) are listed at the top. The DC-8 flight track is indicated in black.

Figure 6. PEM-West B composite meridional cross-section of mixing ratios for (a) C_2H_2/CO and (b) C_3H_8/C_2H_6 for 120°E-140°E longitude. Squares represent the mean of all measured ratios in the area, with the standard deviation listed in italics. Squares with less than 3 data points do not have a listed standard deviation. C_3H_8/C_2H_6 ratio values are multiplied by 100 for clarity in the figure. The dashed line denotes the difference between Case 1 and Cases 2 and 3.

Figure 7. Same as Figure 6, but for 140°E-160°E longitude.

Figure 8. Mean streamlines and wnids (m sec^{-1}) for the PEM-West B mission (February 7 - March 15, 1994) at (a) 850 hPa, (b) 500 hPa, and (c) 300 hPa.

Figure 9. Mean vertical velocity (0.01 Pa sec^{-1}) at 700 hPa for PEM-West B, February 7 - March 15, 1994.

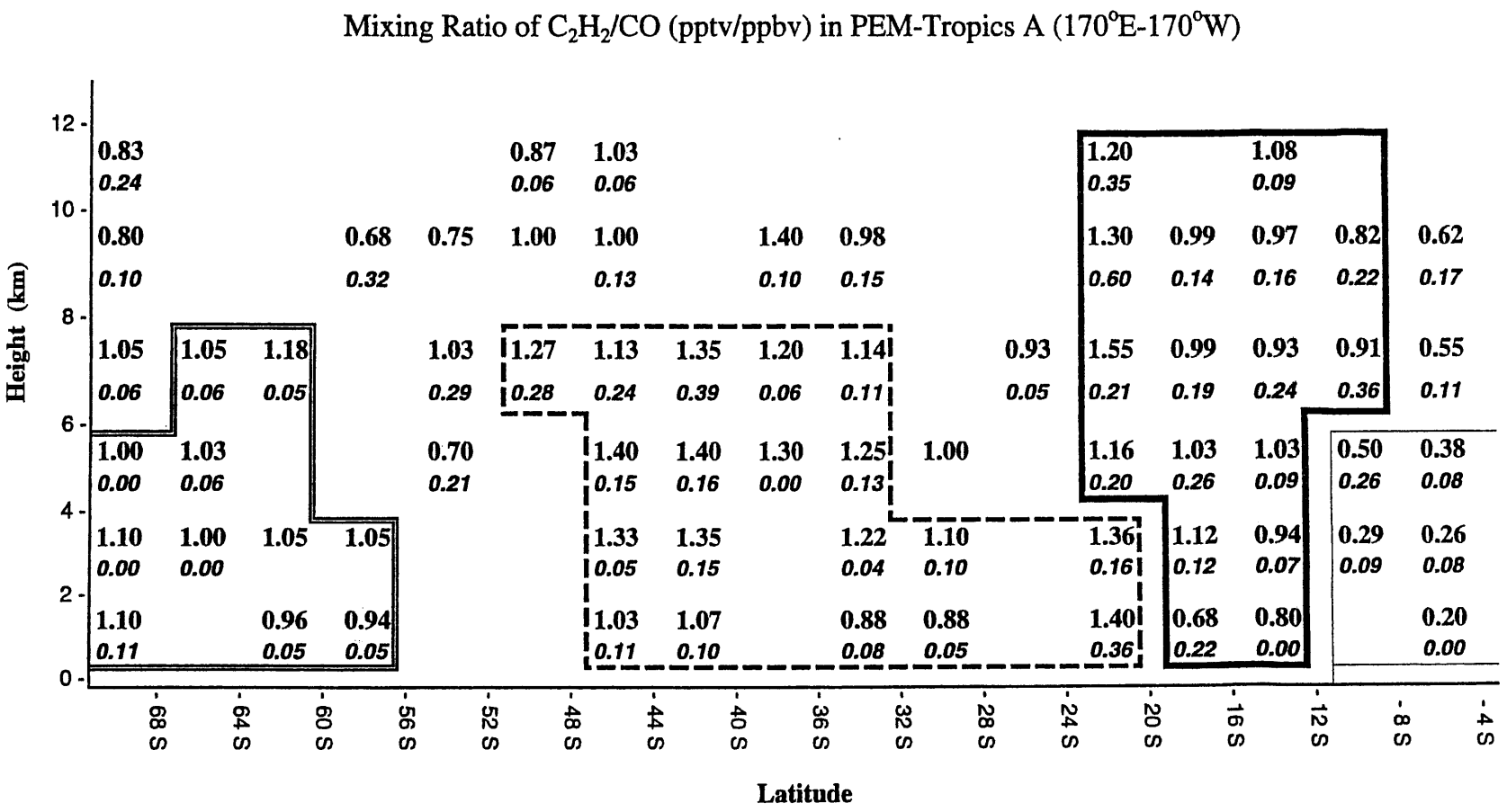
Mixing Ratio of C_2H_2/CO (pptv/ppbv) in PEM-Tropics A (170°E-170°W)
Height (km)
12
10
8
6
4
2
0
0.83 0.24
0.87 1.03 0.06 0.06
1.20 0.35
1.08 0.09
0.80 0.10
0.68 0.32
0.75
1.00 1.00 0.13
1.40 0.10
0.98 0.15
1.30 0.60
0.99 0.14
0.97 0.16
0.82 0.22
0.62 0.17
1.05 0.06
1.05 0.06
1.18 0.05
1.03 0.29
1.27 0.28
1.13 0.24
1.35 0.39
1.20 0.06
1.14 0.11
0.93 0.05
1.55 0.21
0.99 0.19
0.93 0.24
0.91 0.36
0.55 0.11
1.00 0.00
1.03 0.06
0.70 0.21
1.40 0.15
1.40 0.16
1.30 0.00
1.25 0.13
1.00
1.16 0.20
1.03 0.26
1.03 0.09
0.50 0.26
0.38 0.08
1.10 0.00
1.00 0.00
1.05
1.05
1.33 0.05
1.35 0.15
1.22 0.04
1.10 0.10
1.36 0.16
1.12 0.12
0.94 0.07
0.29 0.09
0.26 0.08
1.10 0.11
0.96 0.05
0.94 0.05
1.03 0.11
1.07 0.10
0.88 0.08
0.88 0.05
1.40 0.36
0.68 0.22
0.80 0.00
0.20 0.00
68 S
64 S
60 S
56 S
52 S
48 S
44 S
40 S
36 S
32 S
28 S
24 S
20 S
16 S
12 S
8 S
4 S
Latitude

Figure 1(a)

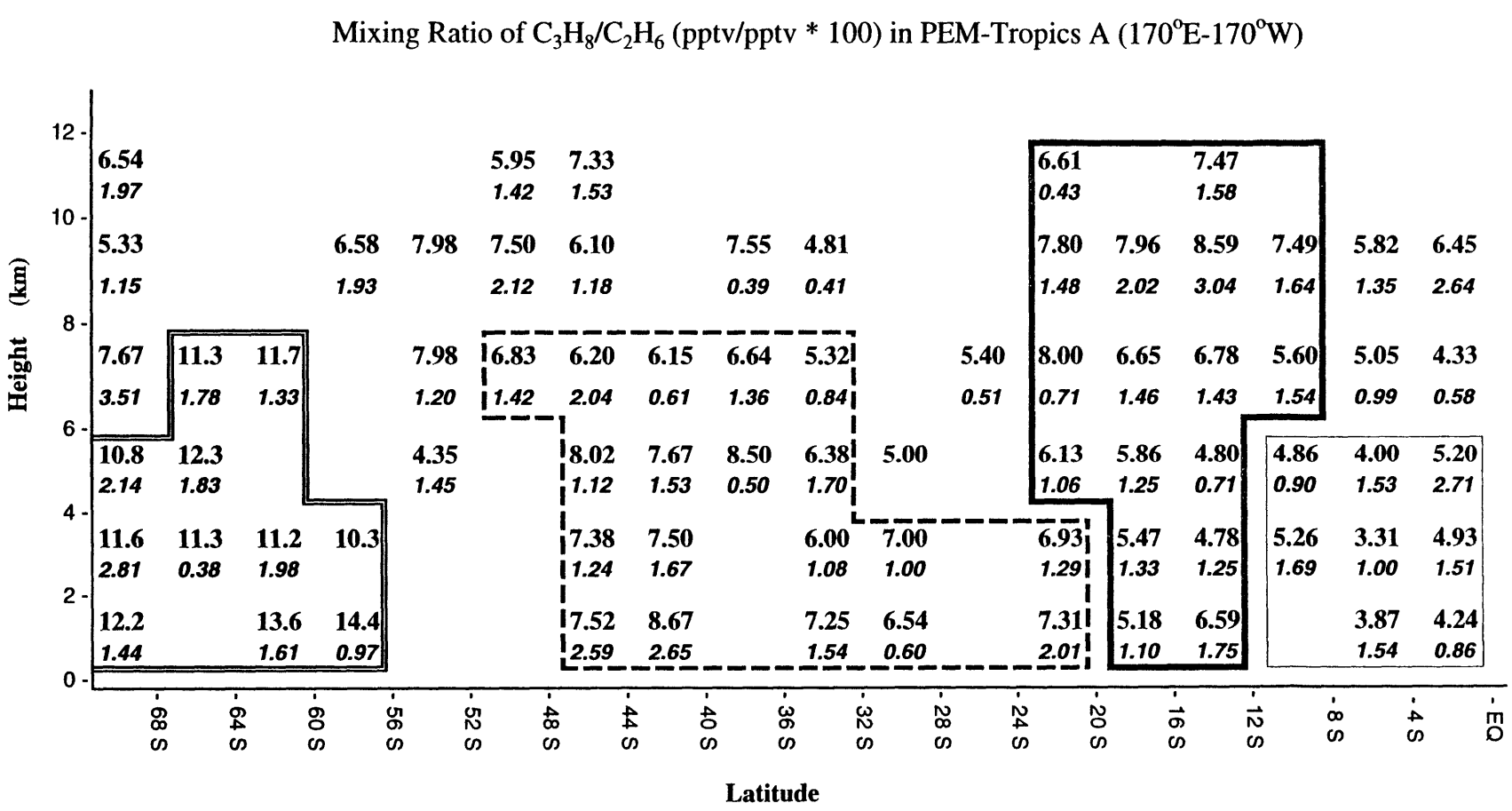
Mixing Ratio of C_3H_8/C_2H_6 (pptv/pptv * 100) in PEM-Tropics A (170°E-170°W)
Height (km)
12
10
8
6
4
2
0
6.54 1.97
5.95 1.42
7.33 1.53
6.61 0.43
7.47 1.58
5.33 1.15
6.58 1.93
7.98
7.50 2.12
6.10 1.18
7.55 0.39
4.81 0.41
7.80 1.48
7.96 2.02
8.59 3.04
7.49 1.64
5.82 1.35
6.45 2.64
7.67 3.51
11.3 1.78
11.7 1.33
7.98 1.20
6.83 1.42
6.20 2.04
6.15 0.61
6.64 1.36
5.32 0.84
5.40 0.51
8.00 0.71
6.65 1.46
6.78 1.43
5.60 1.54
5.05 0.99
4.33 0.58
10.8 2.14
12.3 1.83
4.35 1.45
8.02 1.12
7.67 1.53
8.50 0.50
6.38 1.70
5.00
6.13 1.06
5.86 1.25
4.80 0.71
4.86 0.90
4.00 1.53
5.20 2.71
11.6 2.81
11.3 0.38
11.2 1.98
10.3
7.38 1.24
7.50 1.67
6.00 1.08
7.00 1.00
6.93 1.29
5.47 1.33
4.78 1.25
5.26 1.69
3.31 1.00
4.93 1.51
12.2 1.44
13.6 1.61
14.4 0.97
7.52 2.59
8.67 2.65
7.25 1.54
6.54 0.60
7.31 2.01
5.18 1.10
6.59 1.75
3.87 1.54
4.24 0.86
68 S
64 S
60 S
56 S
52 S
48 S
44 S
40 S
36 S
32 S
28 S
24 S
20 S
16 S
12 S
8 S
4 S
EQ
Latitude

Figure 1(b)

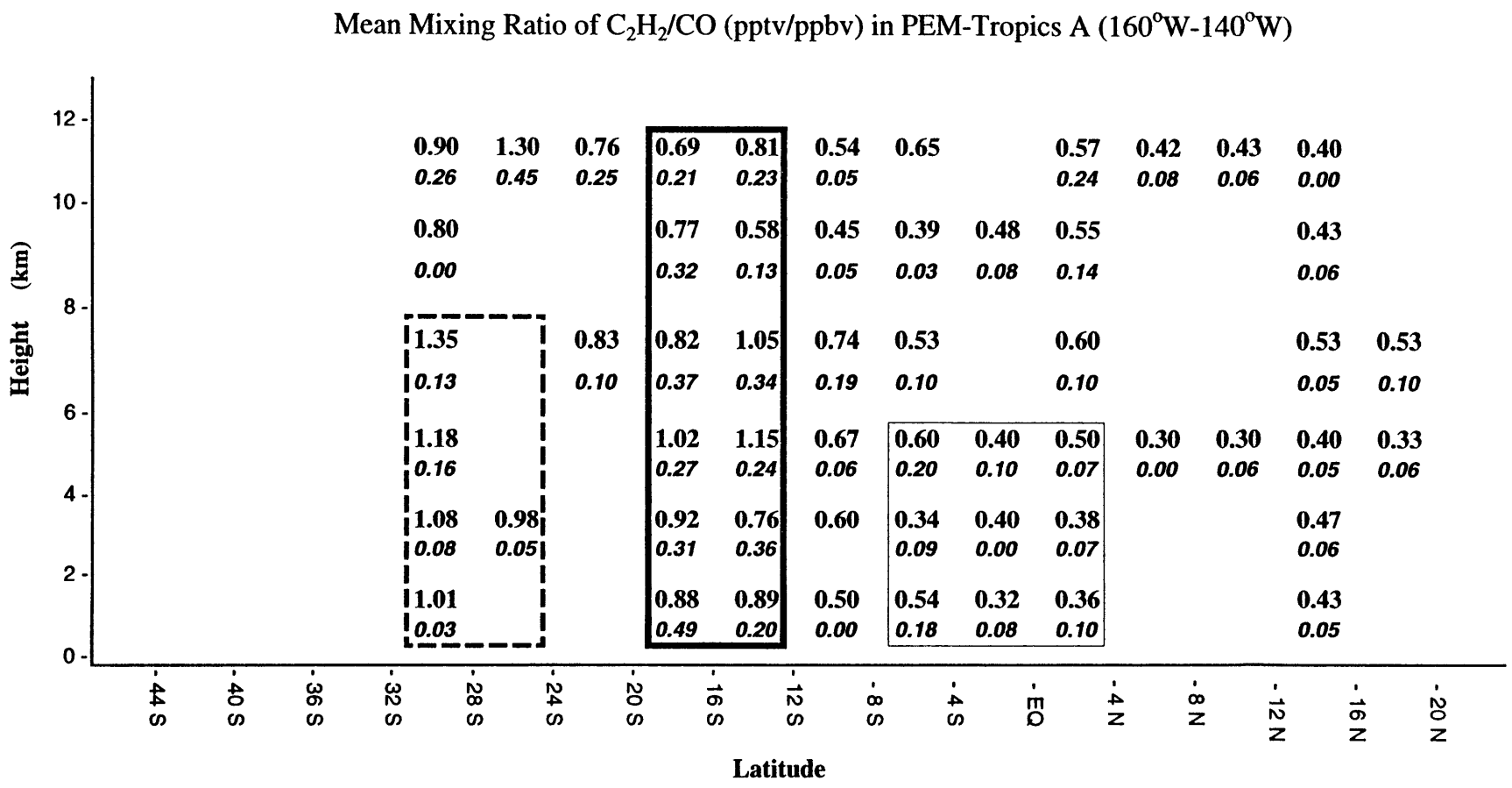
Mean Mixing Ratio of C_2H_2/CO (pptv/ppbv) in PEM-Tropics A (160°W-140°W)
Height (km)
12
10
8
6
4
2
0
0.90 1.30 0.76 0.69 0.81 0.54 0.65 0.57 0.42 0.43 0.40
0.26 0.45 0.25 0.21 0.23 0.05 0.24 0.08 0.06 0.00
0.80 0.77 0.58 0.45 0.39 0.48 0.55 0.43
0.00 0.32 0.13 0.05 0.03 0.08 0.14 0.06
1.35 0.83 0.82 1.05 0.74 0.53 0.60 0.53 0.53
0.13 0.10 0.37 0.34 0.19 0.10 0.10 0.05 0.10
1.18 1.02 1.15 0.67 0.60 0.40 0.50 0.30 0.30 0.40 0.33
0.16 0.27 0.24 0.06 0.20 0.10 0.07 0.00 0.06 0.05 0.06
1.08 0.98 0.92 0.76 0.60 0.34 0.40 0.38 0.47
0.08 0.05 0.31 0.36 0.09 0.00 0.07 0.06
1.01 0.88 0.89 0.50 0.54 0.32 0.36 0.43
0.03 0.49 0.20 0.00 0.18 0.08 0.10 0.05
- 44 S
- 40 S
- 36 S
- 32 S
- 28 S
- 24 S
- 20 S
- 16 S
- 12 S
- 8 S
- 4 S
- EQ
- 4 N
- 8 N
- 12 N
- 16 N
- 20 N
Latitude

Figure 2(a)

Mixing Ratio of C_3H_8/C_2H_6 (pptv/pptv * 100) in PEM-Tropics A (160°W-140°W)

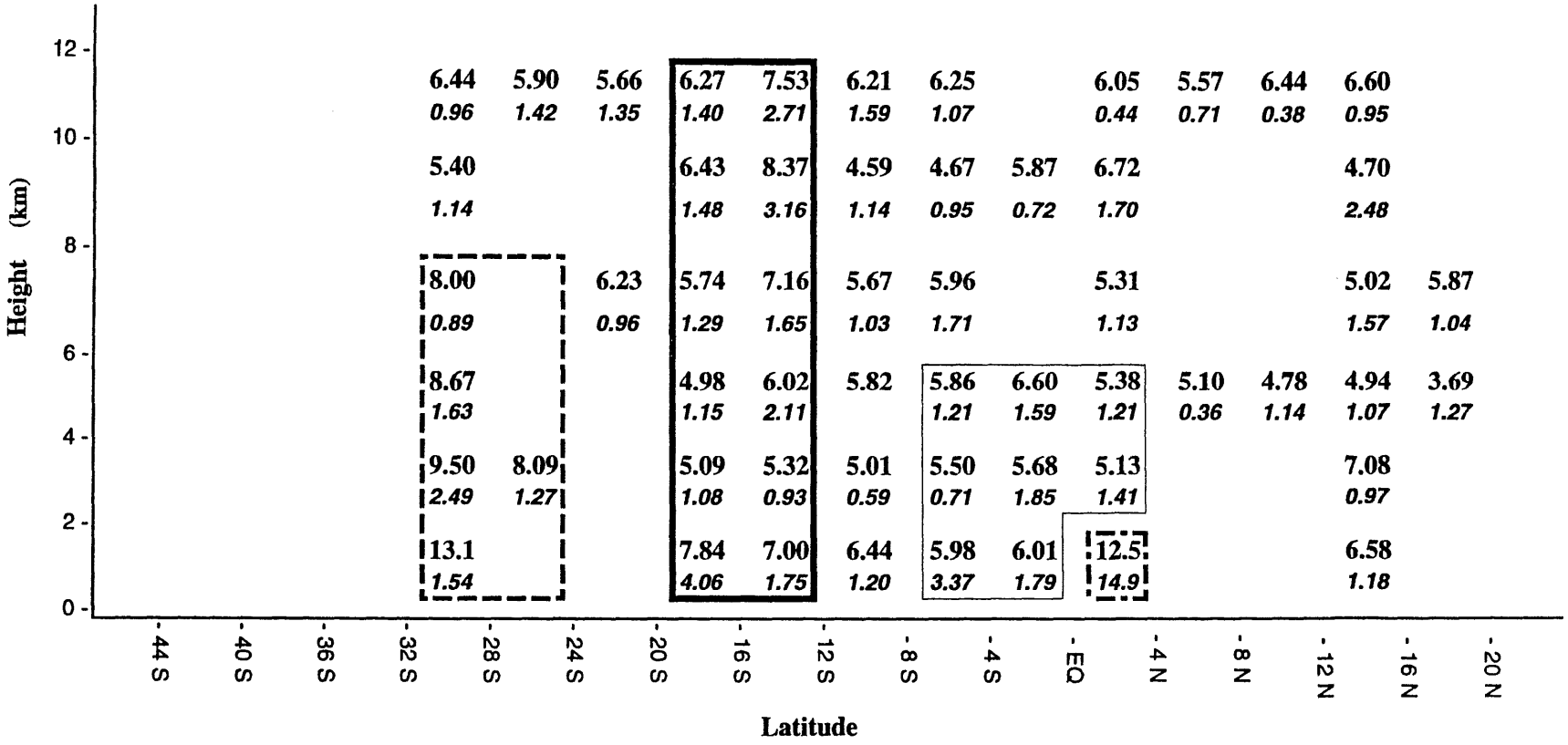

Figure 2(b)

Mean Mixing Ratio of C_2H_2/CO (pptv/ppbv) in PEM-Tropics A (120°W-100°W)

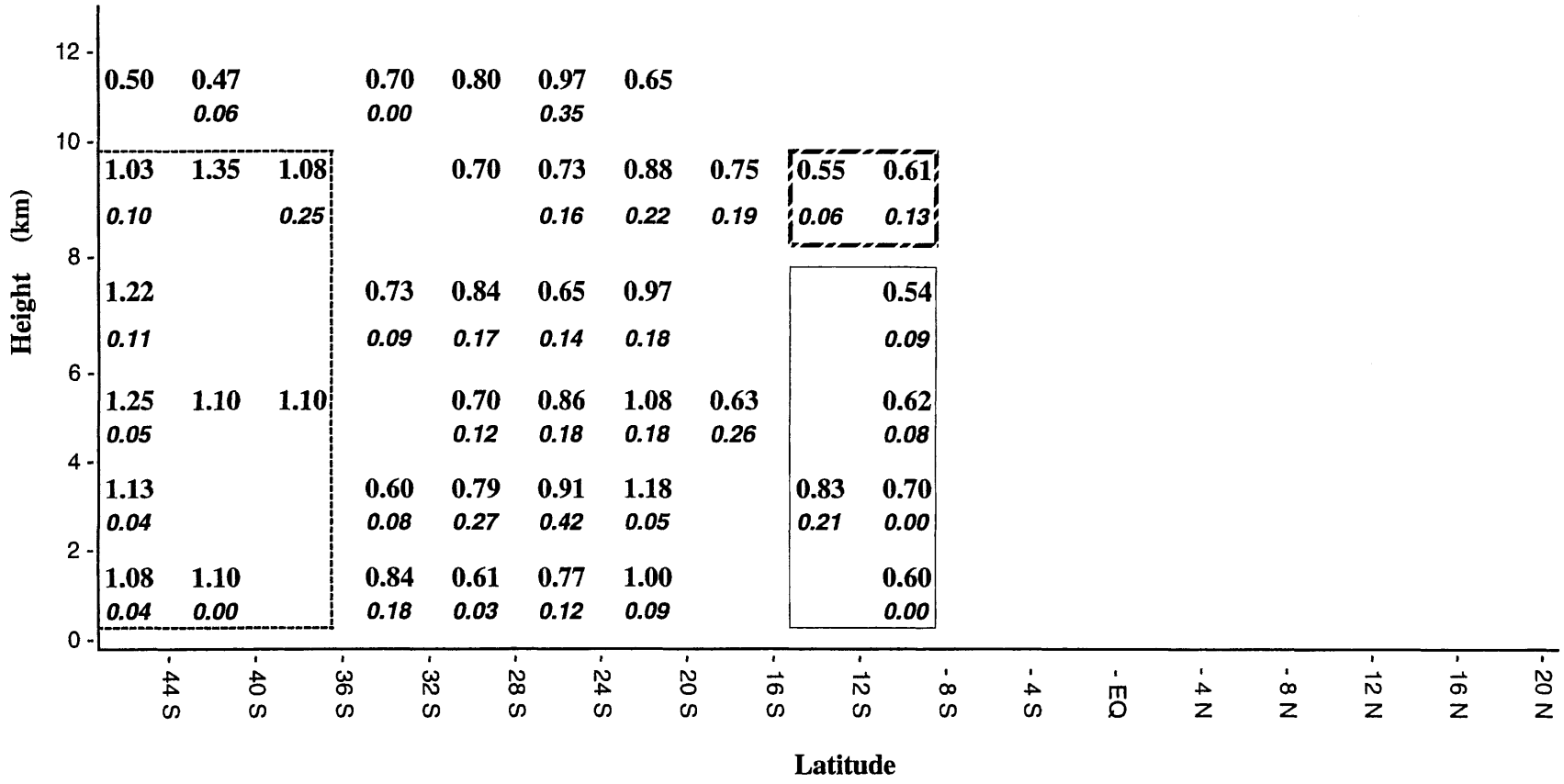

Figure 3(a)

Mixing Ratio of C_3H_8/C_2H_6 (pptv/pptv * 100) in PEM-Tropics A (120°W-100°W)

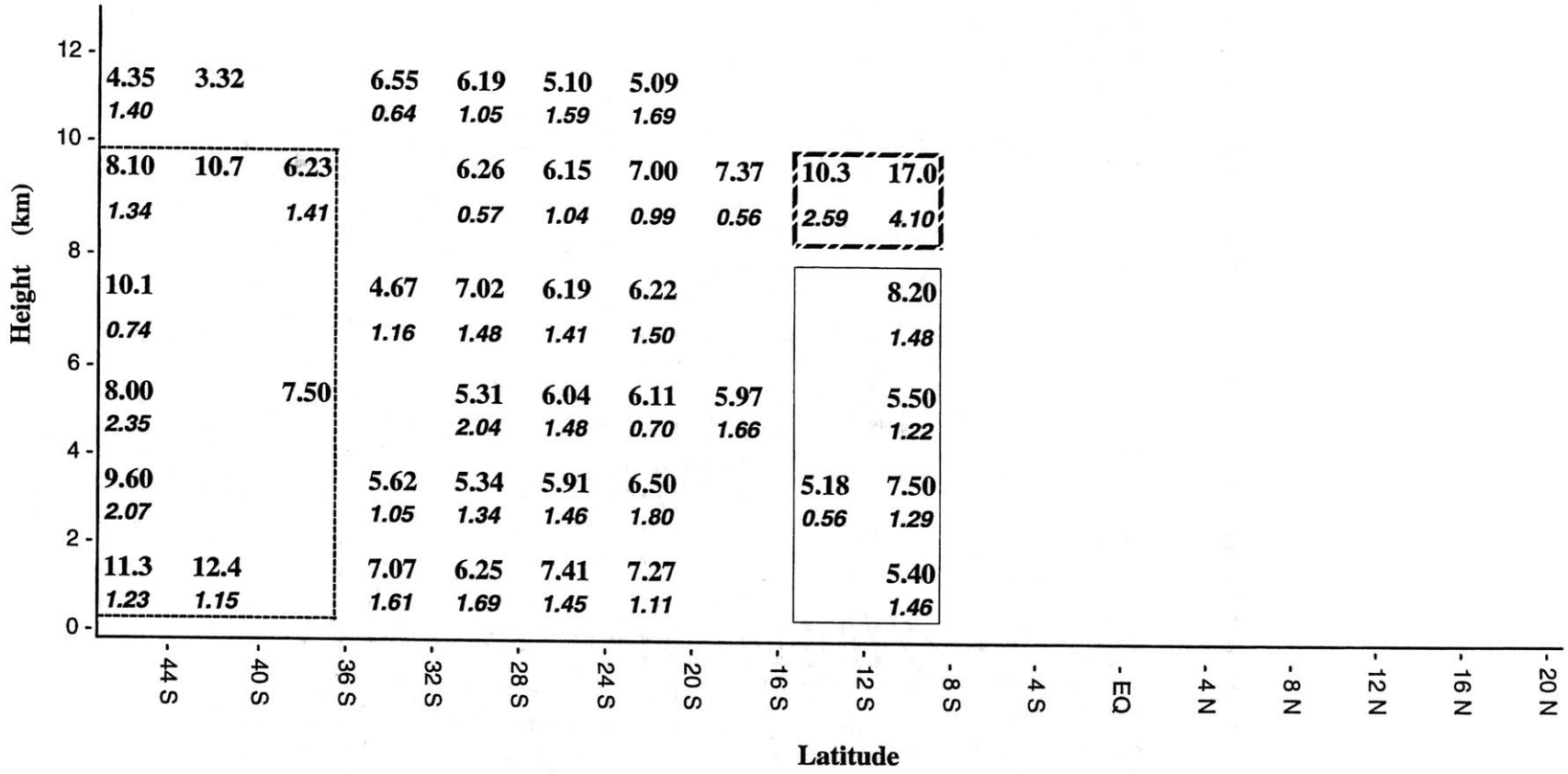

Figure 3(b)

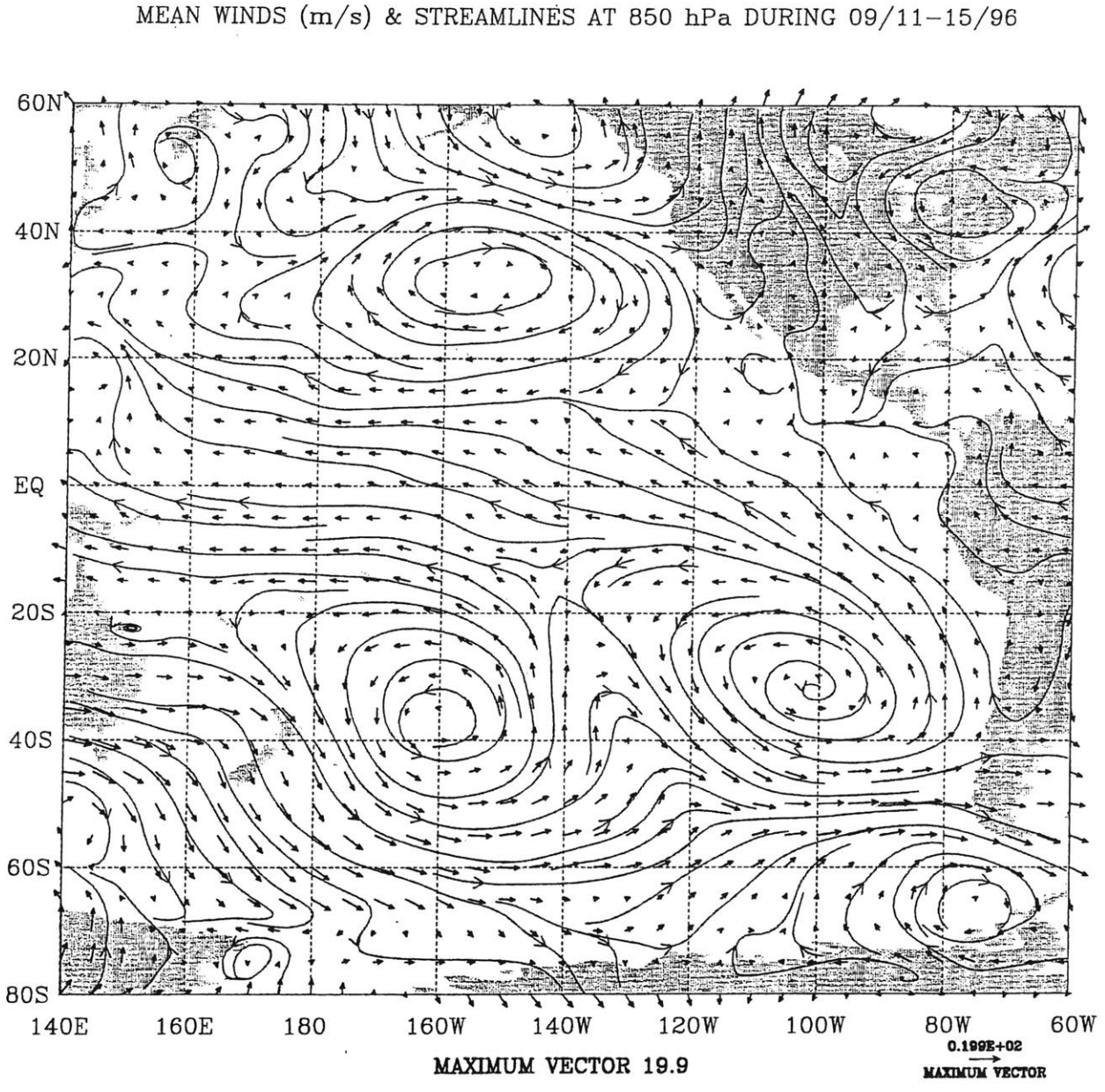
MEAN WINDS (m/s) & STREAMLINES AT 850 hPa DURING 09/11-15/96
60N
40N
20N
EQ
20S
40S
60S
80S
140E
160E
180
160W
140W
120W
100W
80W
60W
MAXIMUM VECTOR 19.9
0.199E+02
MAXIMUM VECTOR

Figure 4(a)

MEAN WINDS (m/s) & STREAMLINES AT 500 hPa DURING 09/11-15/96

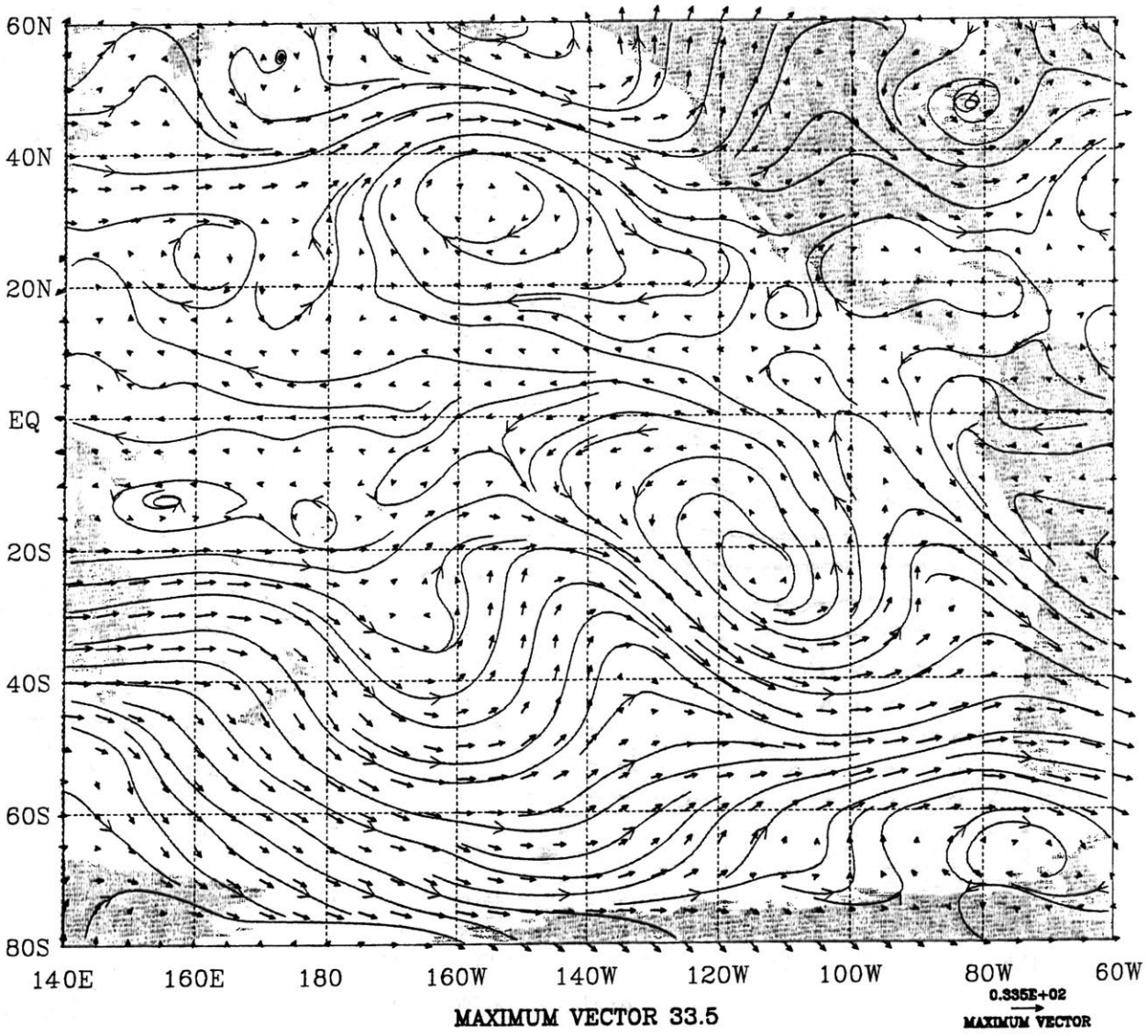

Figure 4(b)

MEAN WINDS (m/s) & STREAMLINES AT 300 hPa DURING 09/11-15/96

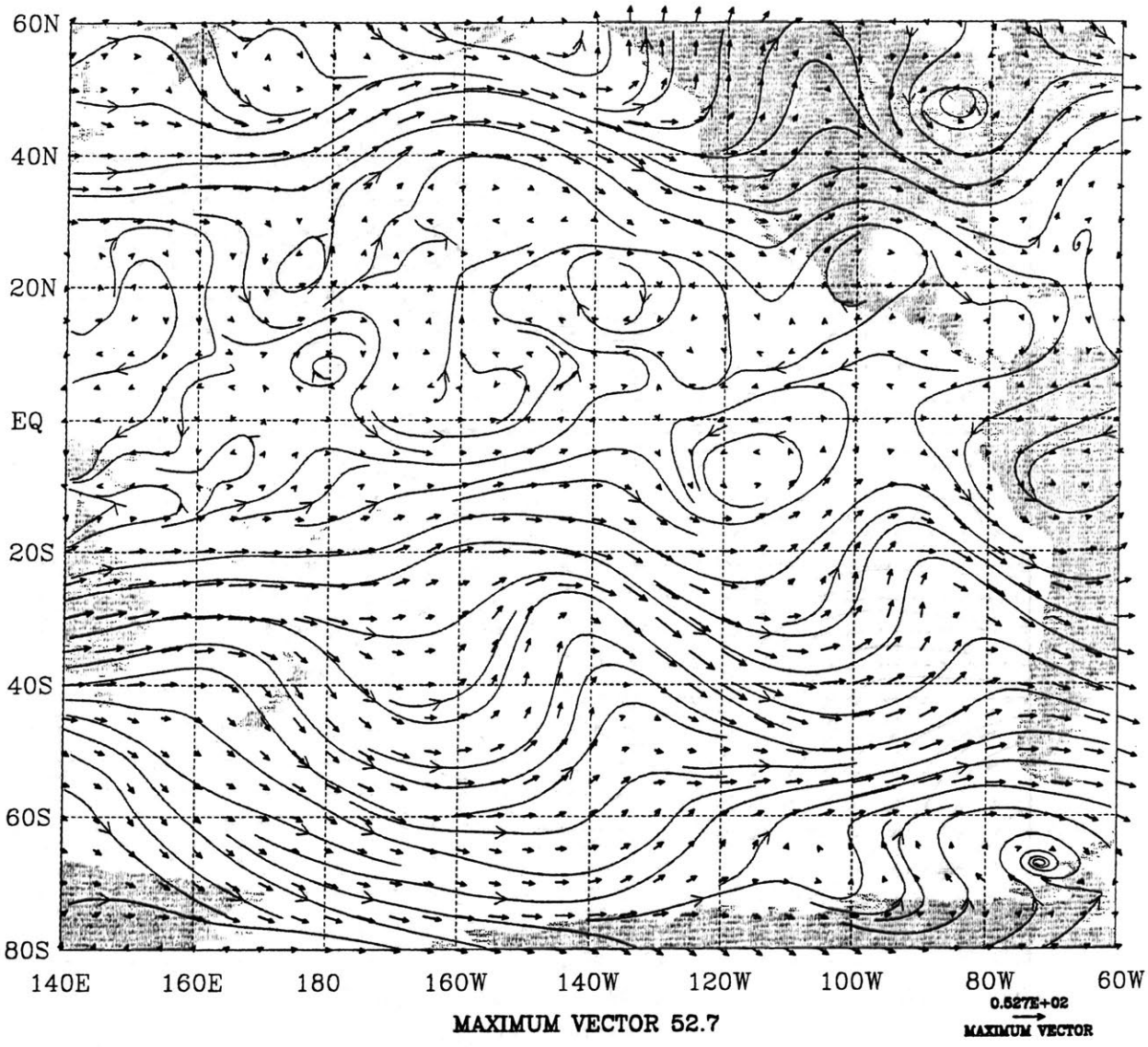

Figure 4(c)

MEAN VERTICAL VELOCITY ON 850 hPa, 11-15/09/96
(UNITS: 0.01 Pa/s)

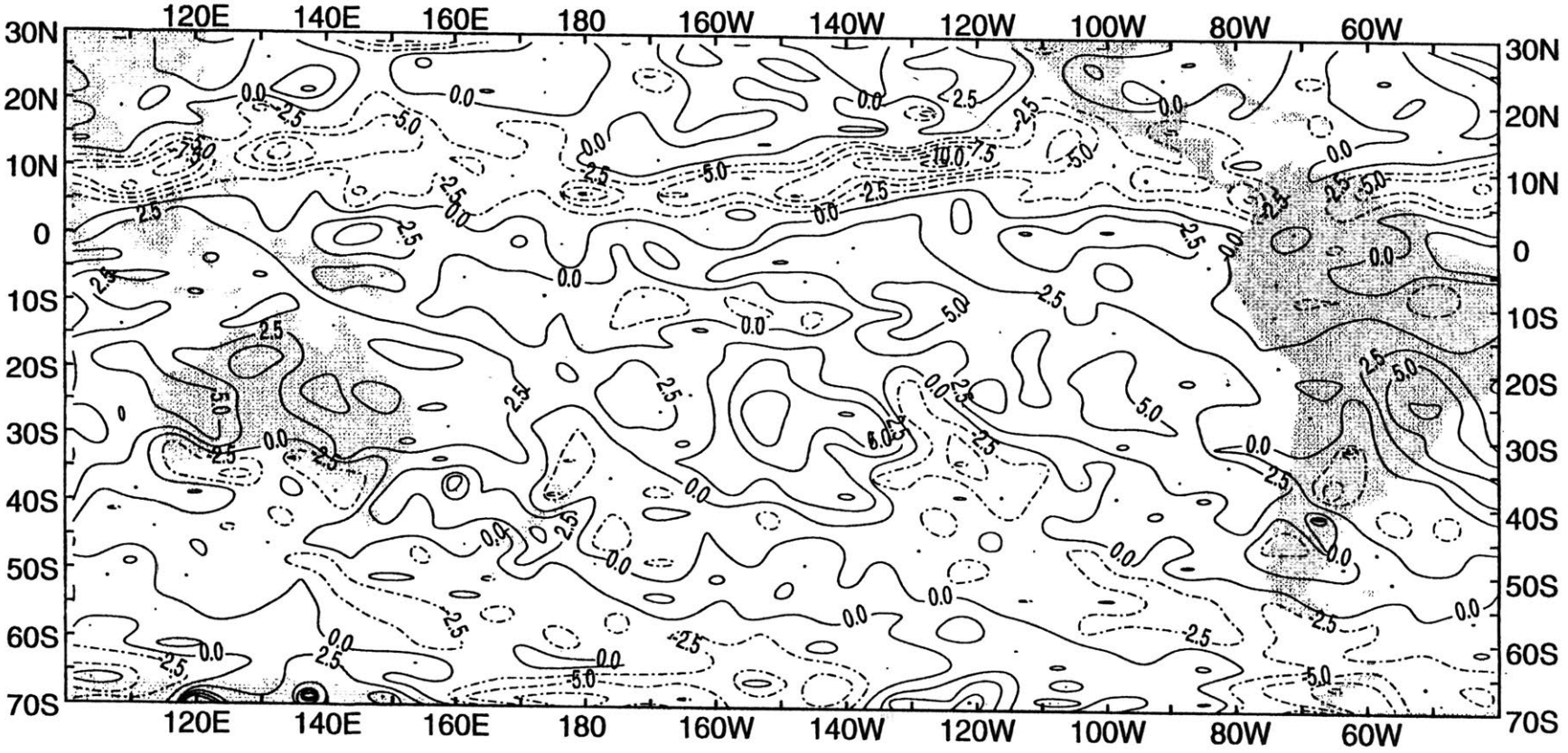

Figure 5

Fiji: SPCZ Gradient Survey

PEM Tropics **Flight 16** **28 Sep 96**

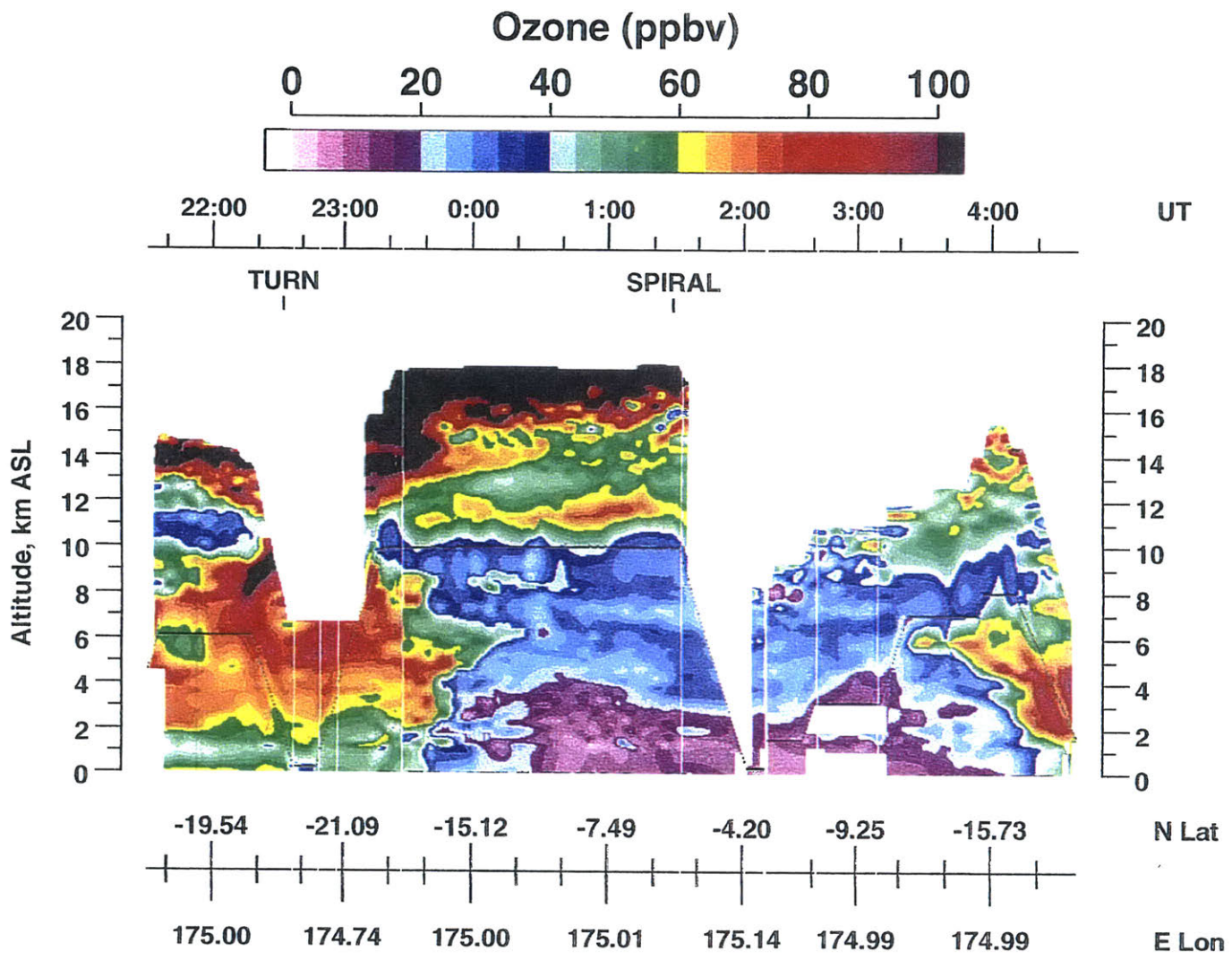

Plate 1

Mixing Ratio of C_2H_2/CO (pptv/ppbv) in PEM-West B (120°E-140°E)

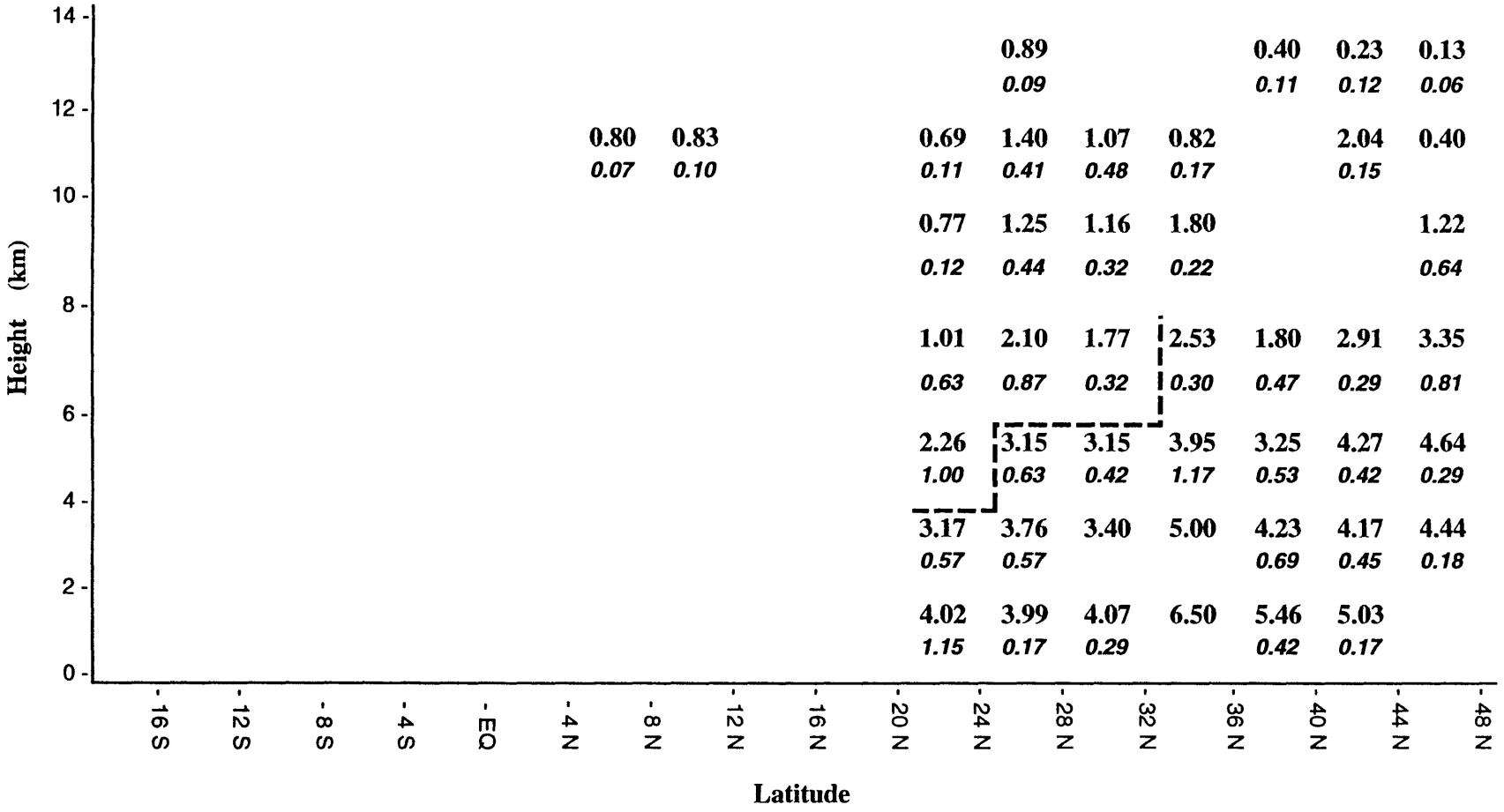

Figure 6(a)

Mixing Ratio of C_3H_8/C_2H_6 (pptv/pptv*100) in PEM-West B (120°E-140°E)

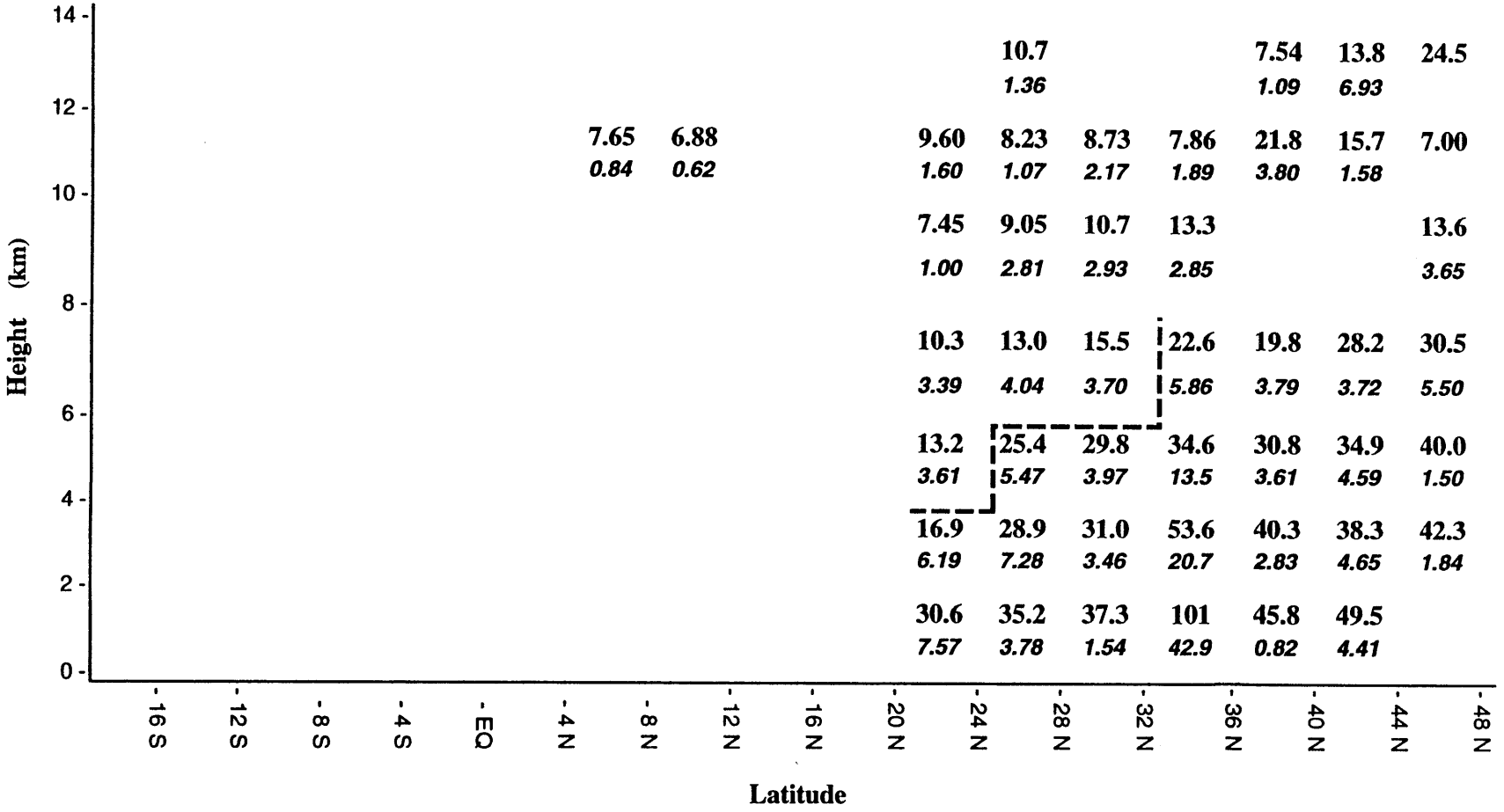

Figure 6(b)

Mixing Ratio of C_2H_2/CO (pptv/ppbv) in PEM-West B (140°E-160°E)

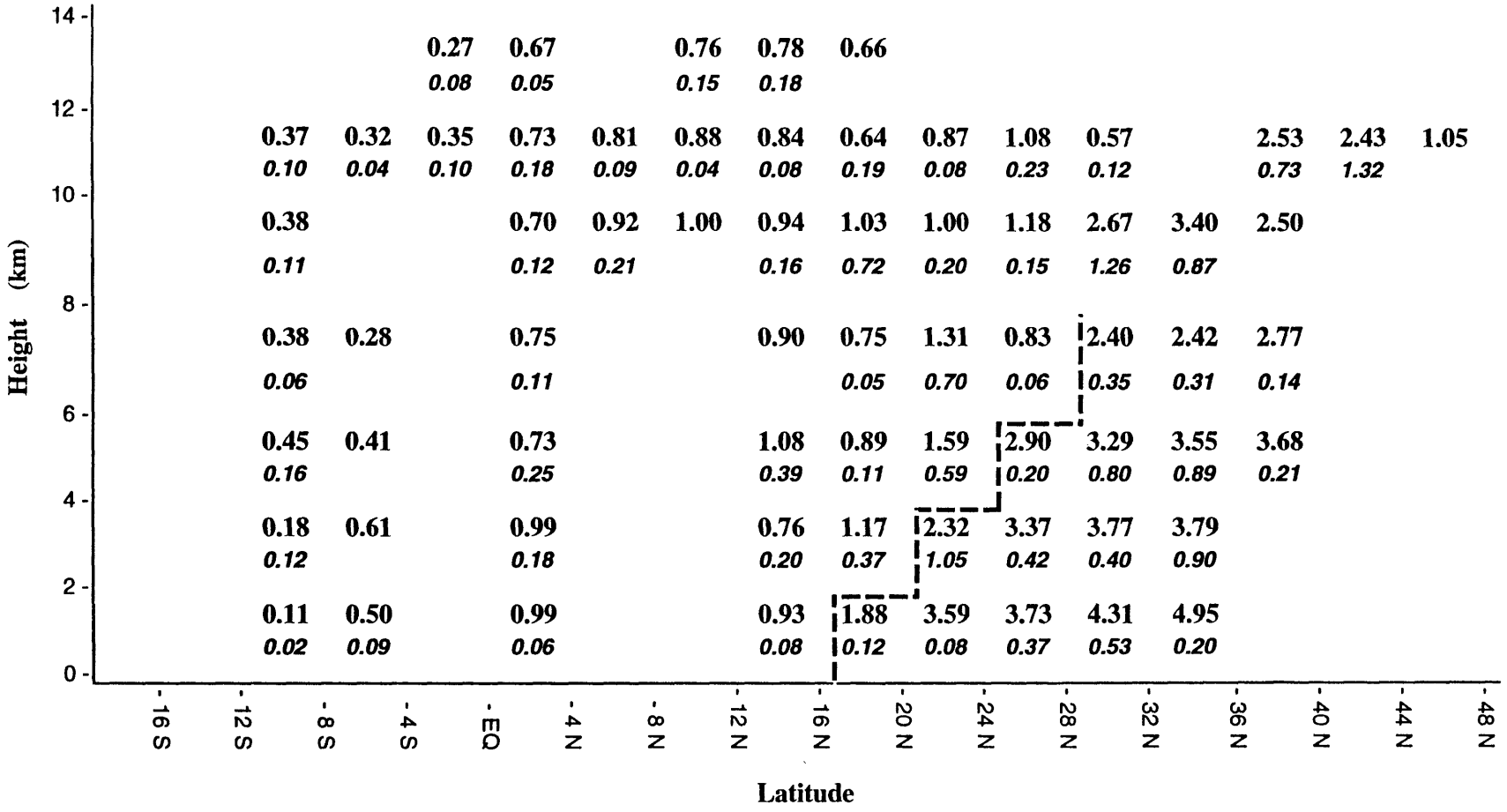

Figure 7(a)

Mixing Ratio of C_3H_8/C_2H_6 (pptv/pptv *100) in PEM-West B (140°E-160°E)

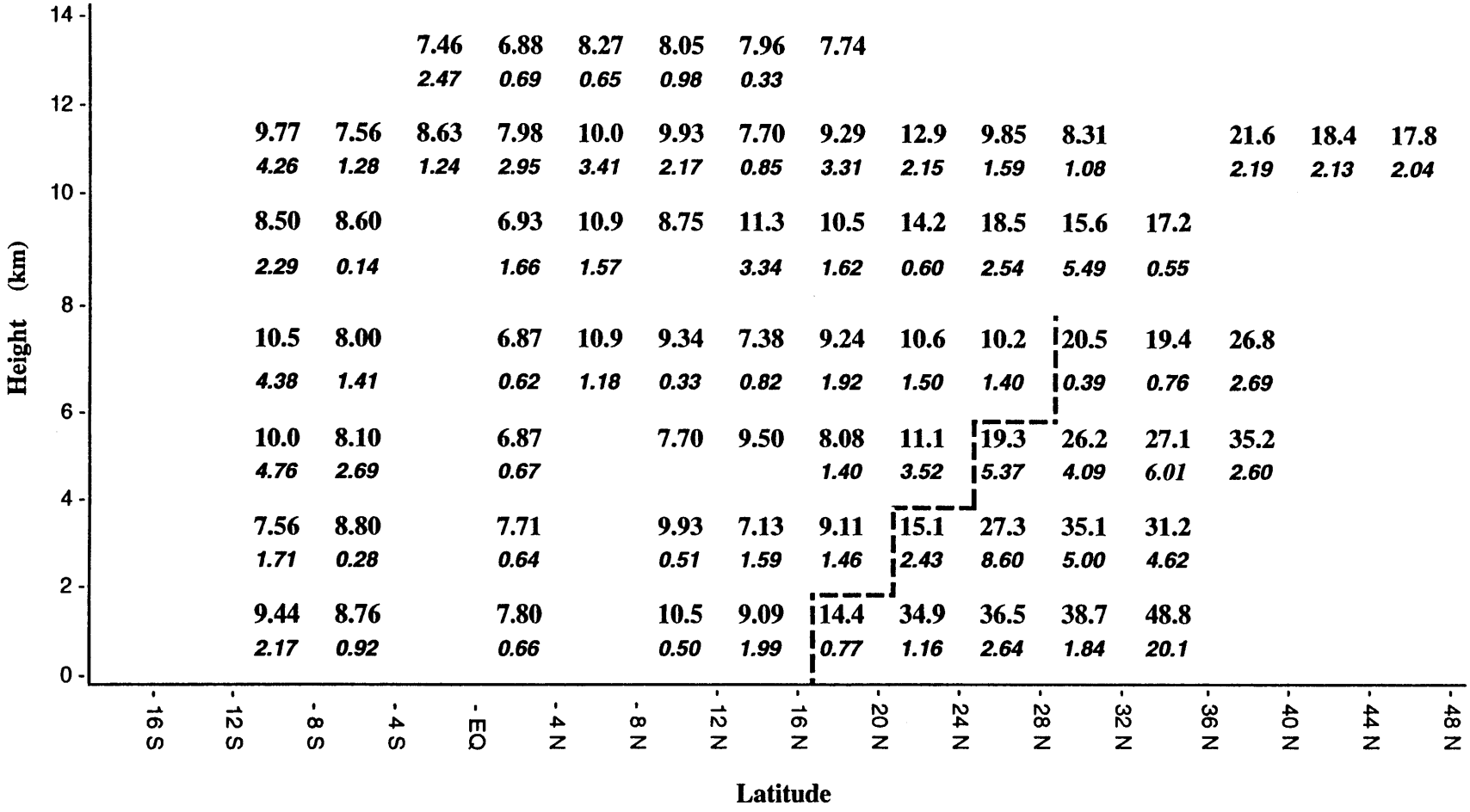

Figure 7(b)

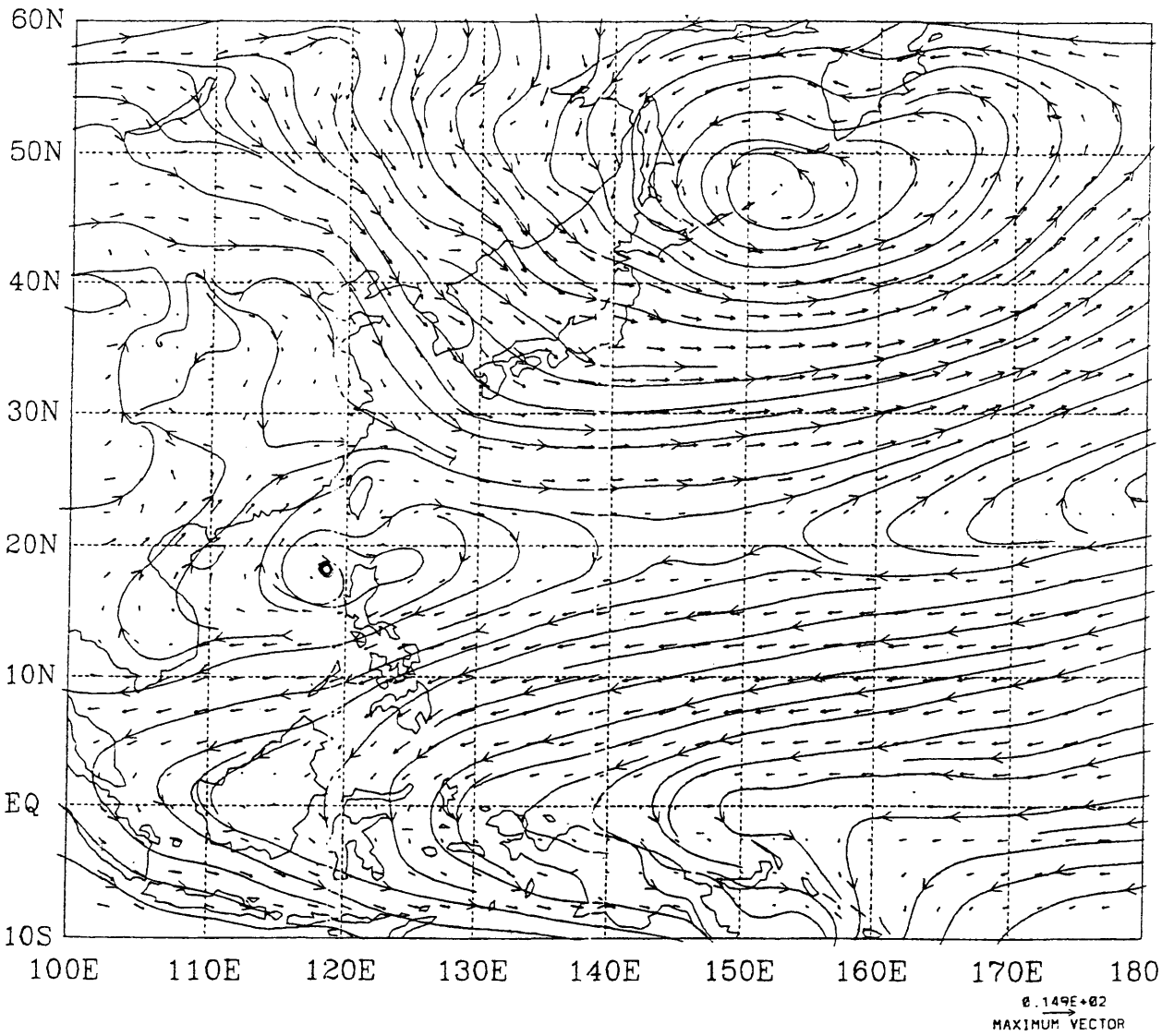
PEMWB MEAN WIND FIELD, WIND VECTOR (m/s) at 850 hPa
60N
50N
40N
30N
20N
10N
EQ
10S
100E
110E
120E
130E
140E
150E
160E
170E
180
0.149E+02
MAXIMUM VECTOR

Figure 8(a)

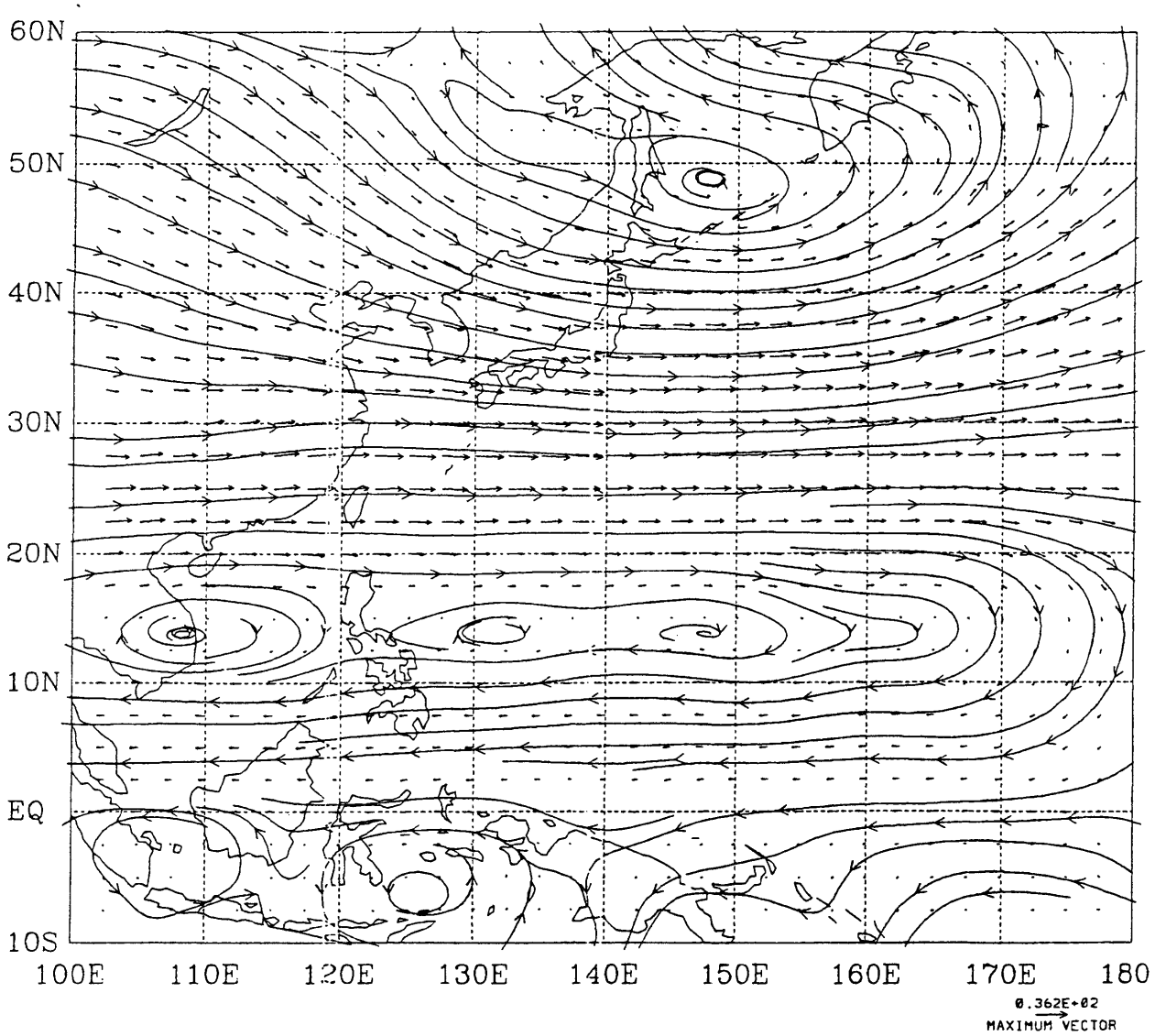
PEMWB MEAN WIND FIELD, WIND VECTOR (m/s) at 500 hPa
60N
50N
40N
30N
20N
10N
EQ
10S
100E
110E
120E
130E
140E
150E
160E
170E
180
0.362E+02
MAXIMUM VECTOR

Figure 8(b)

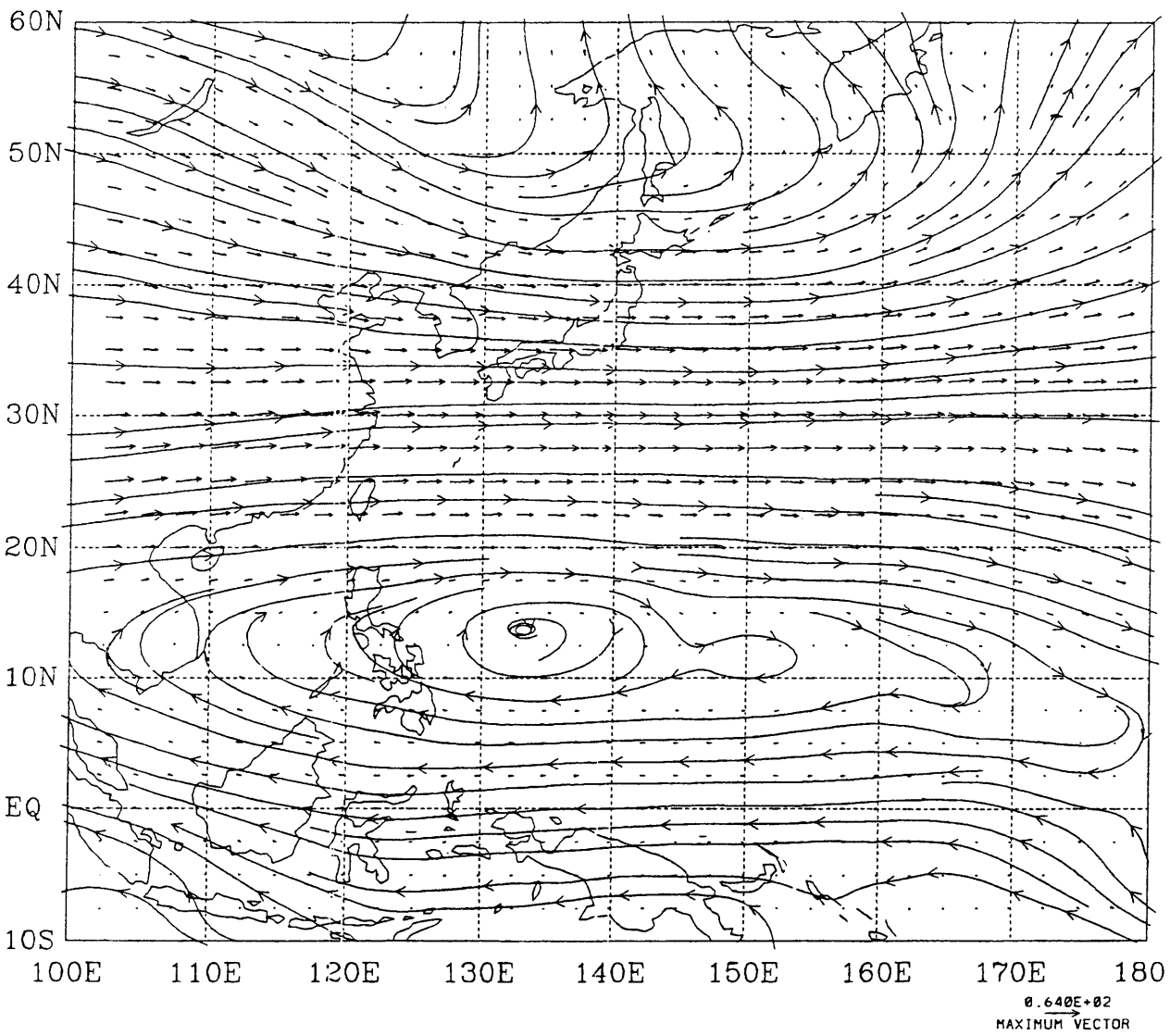
PEMWB MEAN WIND FIELD, WIND VECTOR (m/s) at 300 hPa
60N
50N
40N
30N
20N
10N
EQ
10S
100E
110E
120E
130E
140E
150E
160E
170E
180
0.640E+02
MAXIMUM VECTOR

Figure 8(c)

PEMWB MEAN VERTICAL VELOCITY (0.01 Pa/s) at 700 hPa

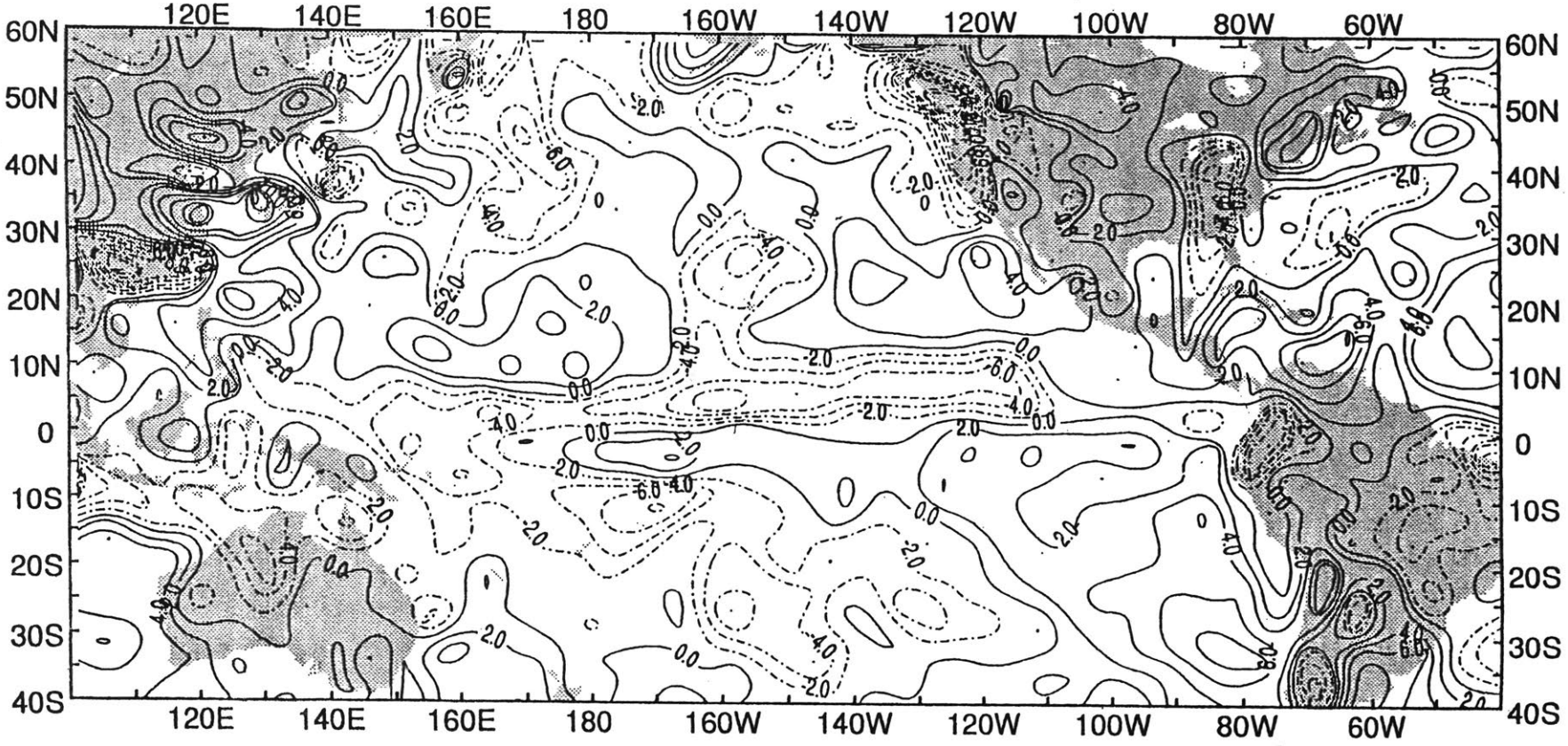

Figure 9